A Dinuclear Nickel Peroxycarbonate Complex: CO$_2$ Addition Promotes H$_2$O$_2$ Release

Hayley L. Lillo and Joshua A. Buss*

Willard Henry Dow Laboratory, Department of Chemistry, University of Michigan, 930 North University Avenue, Ann Arbor, MI 48109, United States

Supporting Information

Experimental

General Considerations:

Unless otherwise specified, all operations were carried out in an MBraun drybox under a nitrogen atmosphere or using standard Schlenk and vacuum line techniques. All reaction glassware for air- and moisture-sensitive chemistry was dried at 140 °C for a minimum of 2 hours and cooled in either an evacuated glovebox antechamber or under vacuum on a Schlenk/vacuum line. Solvents for air- and moisture-sensitive reactions were dried over sodium benzophenone ketyl, calcium hydride, or by the method of Grubbs.[1] Deuterated solvents were purchased from Cambridge Isotope Laboratories and either used as received (CD_2Cl_2 and CD_3CN for benchtop chemistry) or vacuum transferred from CaH_2 (CD_2Cl_2 and CD_3CN for glovebox chemistry). Solvents, once dried and degassed, were vacuum transferred directly prior to use or stored under inert atmosphere over activated 4 Å molecular sieves (Fischer Scientific—activated under dynamic vacuum at 210 °C for 72 hours). $Ni(OTf)_2$ was prepared according to literature procedures.[2] Commercial reagents were purchased from standard vendors and used without further purification unless noted otherwise.

^1H, $^{13}C\{^1H\}$, ^{19}F, and DOSY NMR spectra were recorded on Varian Vnmrs 400, 500, or 700 MHz (PFG PFF AutoX Dual Broadband probe) spectrometers with shifts reported in parts per million (ppm). ^1H and $^{13}C\{^1H\}$ spectra are referenced to reported residual solvent chemical shifts downfield of tetramethylsilane (TMS; 0 ppm).[3] ^{19}F and $^{31}P\{^1H\}$ chemical shifts are referenced internally to the deuterated solvent lock. Multiplicities are abbreviated as follows: s = singlet, d = doublet, t = triplet, q = quartet, and sept = septet. Paramagnetic spectra were measured with 0.2 second acquisition times, 0.1 second relaxation delays, and 160-320 scans per sample in the absence of steady-state scans. The typical acquisition window as amended to 200 to –100 ppm; reported spectra include all resonances observed in this chemical shift range.

Solution IR spectra were recorded on a Thermo Scientific Nicolet iS50 FT-IR spectrometer using a cell equipped with KBr plates and the solvent specified below. The windows were separated by a 0.2 mm Teflon spacer. Solid state IR spectra were recorded on a Thermo Scientific Nicolet iS50 FT-IR spectrometer, using the ATR accessory equipped with a diamond crystal.

UV-Visible spectra were recorded on a Thermo Scientific Evolution Pro UV-Visible spectrometer using a quartz cuvette/cell with a 10 mm path. Spectra were collected from 350 to 800 nm with a 0.07 second integration time, 0.5 nm data interval, 429 nm/min scan speed; a full spectral width scan spanned approximately 79 seconds.

ESI-MS data were collected on an Agilent Technologies 6230 TOF Liquid Chromatography Mass Spectrometer equipped with a 1260 Infinity pump. Samples were introduced via direct infusion as dilute (*ca*. 1 mM) acetonitrile solutions at room temperature.

Synthesis of Li[BPʰBuP] (LiL)
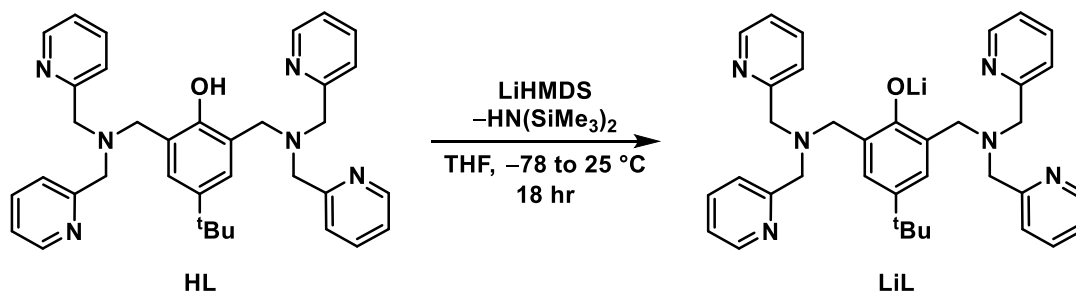
The ligand **H[BPʰBuP] (HL)** was prepared according to a reported literature procedure,[4] affording a tacky off-white solid. Spectra data (^{1}H NMR) matched precedent, with the following salient resonances:

^{1}H NMR (400 MHz, CDCl$_3$, 25 °C) δ (ppm): 10.79 (1H, s), 8.52 (4H, m), 7.61 (4H, m), 7.48 (4H, m), 7.18 (2H, s), 7.10 (4H, m), 3.87 (8H, s), 3.79 (4H, s), 1.28 (9H, s).

A 250 mL Teflon stoppered Schlenk tube was charged with a magnetic stir bar and **HL** (6.83 g, 12.0 mmol, 1.0 equiv.). The flask was evacuated and backfilled with nitrogen three times, leaving the headspace under an active N$_2$ atmosphere. The stopper was replaced with a rubber septum and dry THF (40 mL) was admitted via cannula, affording a pale amber solution. The Schlenk tube was cooled to −78 °C in a dry ice/acetone bath and stirring was initiated. A THF solution (20 mL) of LiHMDS (2.00 g, 12.0 mmol, 1.0 equiv.), was added dropwise over the course of approximately twenty minutes, and the solution gradually adopted a pale pink/red hue. The septum was replaced with a Teflon stopper, the cooling bath was removed, and the reaction mixture was allowed to warm to room temperature slowly. Stirring continued for 18 hours, at which time, the reaction volatiles were removed under reduced pressure. The resultant solids were taken up in diethyl ether (40 mL) and left to stand at −35 °C overnight, precipitating off-white solids. This mixture was filtered through a medium porosity sintered glass frit. The solids were washed with minimal diethyl ether (*ca*. 5 mL), collected, and dried under reduced pressure to yield **LiL** as an ivory powder (6.64 g, 11.5 mmol, 96%). The purity of this phenolate salt was established via proton NMR spectroscopy in proteo 1,4-dioxane with solvent suppression.

^{1}H NMR (400 MHz, C$_4$O$_2$H$_8$, 25 °C) δ (ppm): 8.26 (4H, dd, J = 6.5 & 4.9 Hz), 7.36 (4H, dd, J = 12.4 & 5.9), 7.26 (4H, dd, J = 6.5 & 6.2 Hz), 7.02 (2H, s), 6.87 (4H, dd, J = 12.4 & 5.8 Hz), 1.19 (9H, s).

^{13}C{^{1}H} NMR (151 MHz, C$_4$O$_2$H$_8$, 25 °C) δ (ppm) 166.66, 161.40, 150.22, 137.17, 132.49, 126.34, 125.31, 123.36, 122.62, 61.41, 34.63, 33.05.

Note: The benzylic methylene protons coincide with the solvent-suppressed 1,4-dioxane solvent residual in both the ^{1}H and ^{13}C{^{1}H} spectra.

Note: The satellites surrounding the 1,4-dioxane solvent residual (δ = 77.94, 73.99, 73.00, 71.03, 70.05, 68.06, 66.10, 65.10, 63.14, 62.15, and 58.20 ppm) were corroborated as such via collection of a ^{13}C{^{1}H} spectrum of authentic solvent.
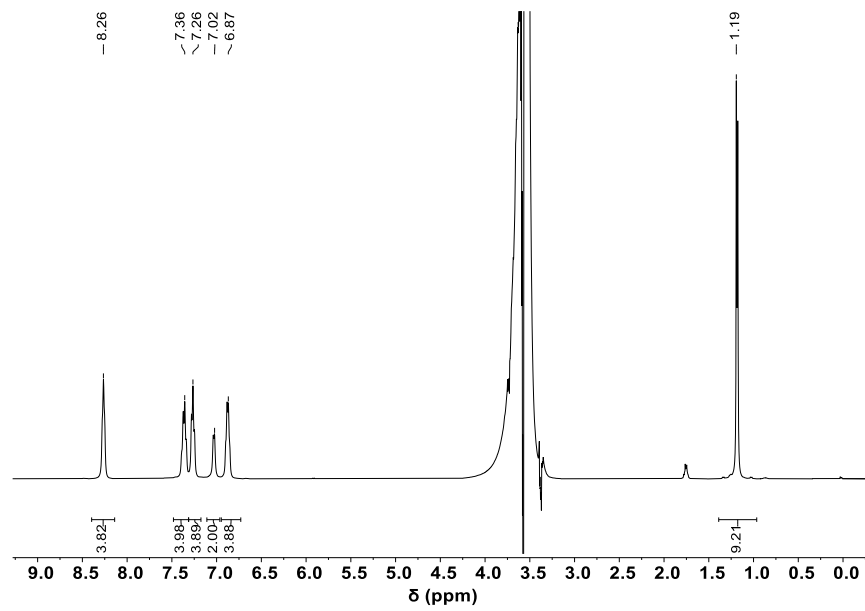
Figure S1. ^{1}H NMR spectrum of **LiL** ($C_4O_2H_8$, 25 °C, 400 MHz).
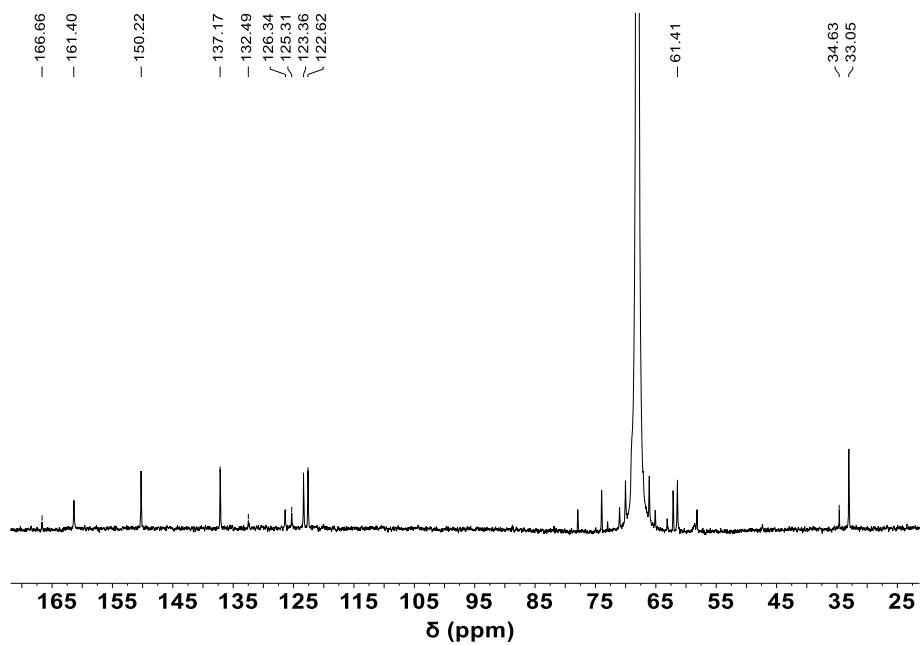
Figure S2. ^{13}C{^{1}H} NMR spectrum of **LiL** ($C_4O_2H_8$, 25 °C, 151 MHz).

Synthesis of [LNi₂(OTf)₂][OTf]
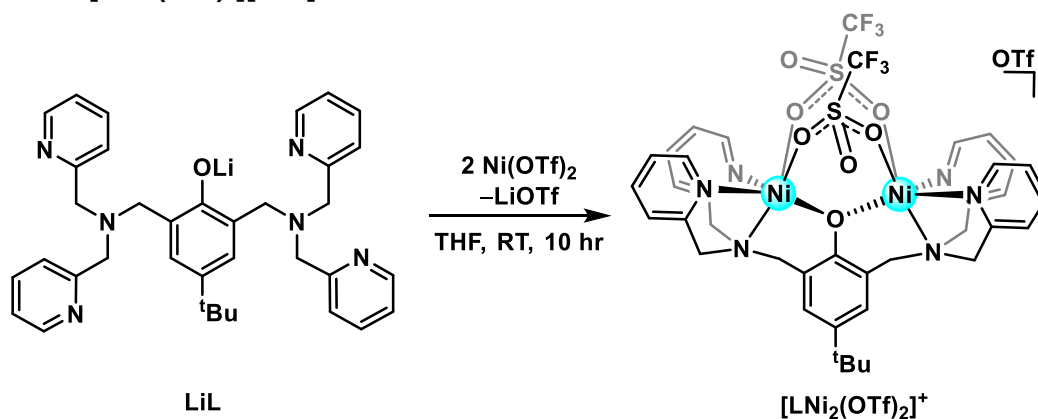
In the glovebox, a 100 mL round bottom flask was charged with **LiL** (520 mg, 0.91 mmol, 1.0 equiv.), Ni(OTf)₂ (651 mg, 1.83 mmol, 2.0 equiv.), and a magnetic stir bar. THF (35 mL) was added, and the resultant teal-blue solution was stirred for 10 hours. At this time, the reaction volatiles were removed under reduced pressure, yielding a pale blue powder. Subsequent sequential trituration with hexanes (2 x 2 mL), diethyl ether (2 x 2 mL), and benzene (2 x 2 mL) provided a deep blue powder. The solids were suspended in benzene (*ca.* 5 mL) and filtered through a pad of Celite on a sintered glass frit. The filter cake was extracted with THF until the filtrate ran colorless (*ca.* 20 mL) and the THF filtrate was dried *in vacuo*, affording **[LNi₂(OTf)₂]⁺** as a light blue free-flowing powder (942 mg, 0.83 mmol, 91% yield). X-ray quality single crystals were grown by layering a concentrated DCM solution with diethyl ether and allowing slow admixture of the layers at –35 °C. Thin blue needles were observed to form after approximately 48 hours.

^{1}H NMR (400 MHz, CD₂Cl₂) δ (ppm): 156.84, 136.01, 129.94, 121.20, 45.33, 39.72, 36.88, 17.74, 13.74, 13.74, 13.74, 13.09, 8.73, 7.58, 7.23, 6.99.

^{19}F NMR (471 MHz, CD₂Cl₂) δ (ppm): 0.81, –74.42.

UV-Visible Spectrum: λ (nm) 595 (ε = 22 M⁻¹cm⁻¹).

ESI MS. [LNi₂(OTf)₂]⁺: calc. 985.0923; exp. 985.0959 m/z.

Elemental Analysis: Calcd. for **[LNi₂OTf₂][OTf]·0.5CH₂Cl₂** (C₃₉.₅H₄₀ClF₉N₆Ni₂O₁₀S₃) C 40.25%, H 3.42%, N 7.13%; found C 40.29%, H 3.48%, N 7.10%.

Note: Elemental analysis was consistent with a dichloromethane solvate that was likewise observed in the single crystal X-ray diffraction structure.
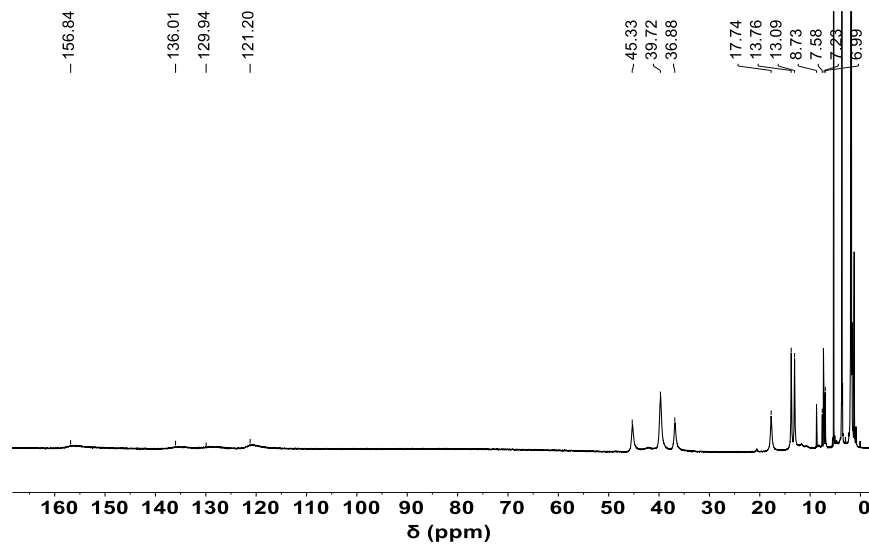
Figure S3. ^{1}H NMR spectrum of **[LNi$_2$(OTf)$_2$]$^+$** (CD$_2$Cl$_2$, 25 °C, 400 MHz).
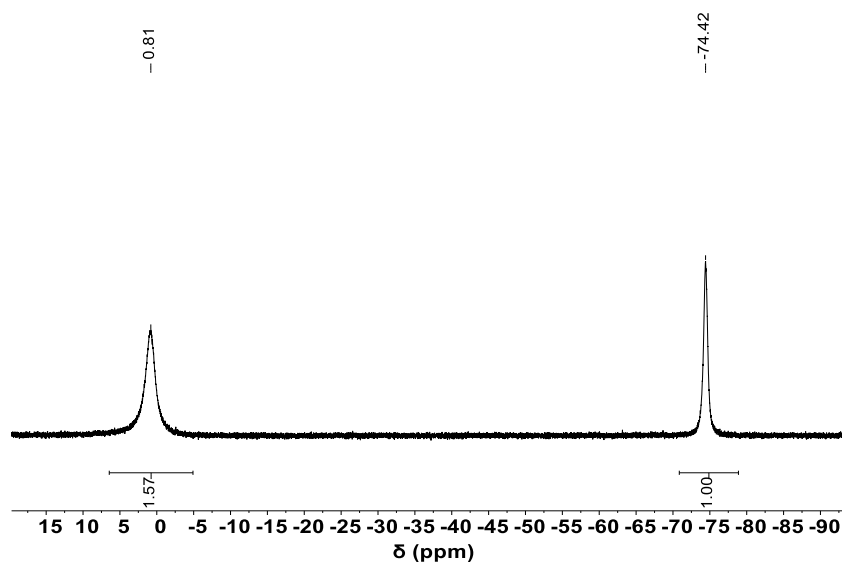
Figure S4. ^{19}F NMR spectrum of **[LNi$_2$(OTf)$_2$]$^+$** (CD$_2$Cl$_2$, 25 °C, 471 MHz).
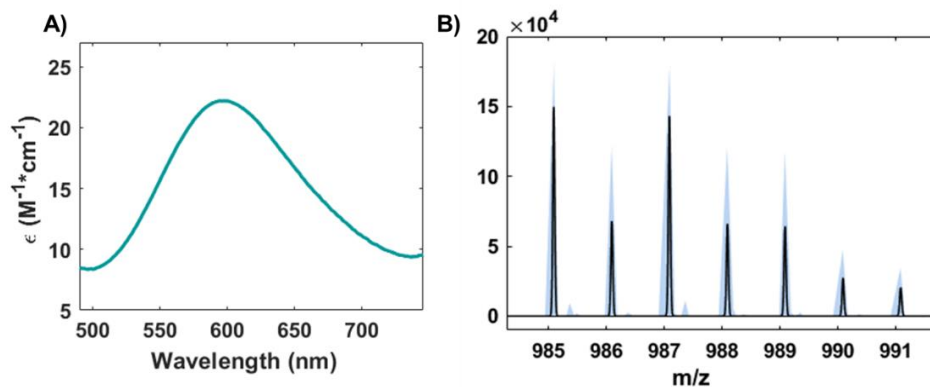
Figure S5. A) UV-visible spectrum of **[LNi$_2$(OTf)$_2$]$^+$** (0.03 mM, 25 °C) in acetonitrile. **B)** Simulated (□) vs. experimental (■) ESI mass spectrum of **[LNi$_2$(OTf)$_2$]$^+$**.

Synthesis of [L$_2$Ni$_4$(CO$_3$)$_2$(H$_2$O)$_2$][OTf]$_2$

[LNi$_2$(OTf)$_2$]$^+$

Method A) 2 NaOH
H$_2$O/MeCN, 25 °C, 18 h

Method B) 2 Na$_2$CO$_3$
MeCN, 25 °C, 18 h

[L$_2$Ni$_4$(CO$_3$)$_2$(H$_2$O)$_2$]$^{2+}$
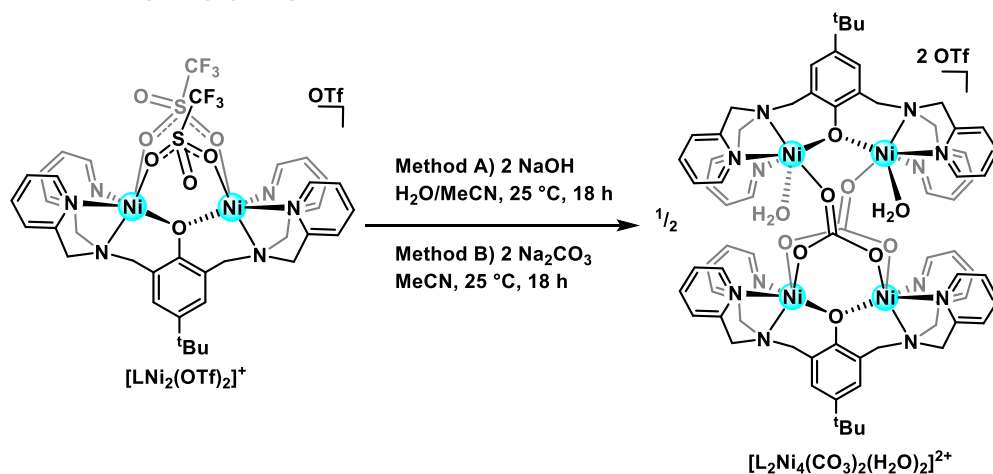
A) A 20 mL scintillation vial was charged with **[LNi$_2$(OTf)$_2$]$^+$** (300 mg, 0.26 mmol, 1.0 equiv.), NaOH (21 mg, 0.53 mmol, 2.0 equiv.), acetonitrile (*ca.* 3 mL), and a magnetic stir bar. In the fume hood, water (*ca.* 3 mL) was added to fully dissolve the NaOH, and the mixture was stirred vigorously for 12 hrs. Reaction volatiles were removed under reduced pressure, and the resulting oily residue was suspended in DCM (*ca.* 2 mL). The mixture was filtered through a Celite plug and the reaction residue and filter cake were further extracted with DCM (2 mL x 3) until the washes ran colorless. The combined filtrate was dried under reduced pressure, affording pale blue solids that were further triturated with hexanes (*ca.* 2 mL). The now free-flowing solids were crystallized via layering a concentrated acetonitrile solution with an equal volume of diethyl ether at room temperature. Microcrystals obtained this way were still not spectroscopically pure; recrystallizing this material through a second acetonitrile/diethyl ether layering afforded analytically pure **[L$_2$Ni$_4$(CO$_3$)$_2$(H$_2$O)$_2$]$^{2+}$** (56 mg, 0.03 mmol, 23% yield).

B) In the fume hood, a 100 mL round bottom was charged with **[LNi$_2$(OTf)$_2$]$^+$** (1.0 g, 0.88 mmol, 1.0 equiv.), Na$_2$CO$_3$ (106 mg, 1.76 mmol, 2.0 equiv.), acetonitrile (35 mL), and a magnetic stir bar. The reaction was heated to 45 °C in an oil bath and left to stir overnight. The solution was left to cool to room temperature, and then filtered through a medium porosity frit. The filtrate was dried under reduced pressure and triturated with a 1:1 mixture of diethyl ether and pentanes (*ca.* 6 mL total). The light blue free-flowing solids were crystallized via vapor diffusion of diethyl ether into a concentrated DCM solution. The resultant microcrystals proved impure but recrystallizing these solids via DCM/diethyl ether vapor diffusion provided analytically pure **[L$_2$Ni$_4$(CO$_3$)$_2$(H$_2$O)$_2$]$^{2+}$** (370 mg, 0.20 mmol, 46% yield). X-ray quality crystalline light blue plates were grown as from DCM and hexanes slowly diffusing into toluene.

^{1}H NMR (500 MHz, CD$_2$Cl$_2$) δ (ppm): 178.79, 171.31, 141.32, 132.09, 128.71, 117.47, 113.54, 106.11, 102.87, 43.67, 42.62, 40.86, 40.42, 40.07, 39.12, 38.83, 37.77, 36.70, 34.74, 22.88, 18.41, 13.20, 12.96, 11.30, 9.84, 1.96, 1.77.

^{19}F NMR (471 MHz, CD$_2$Cl$_2$) δ (ppm): −79.28.

UV-Visible: λ (nm) 594 (ε = 18 M^{-1}cm^{-1}).

ESI MS. [L$_2$Ni$_4$(CO$_3$)$_2$(H$_2$O)$_2$]$^{2+}$ calc. 749.1727; exp. 749.1715 m/z.

Elemental Analysis: Calcd. for **[L$_2$Ni$_4$(CO$_3$)$_2$(H$_2$O)$_2$][OTf]$_2$·10H$_2$O** (C$_{76}$H$_{102}$F$_6$N$_{12}$Ni$_4$O$_{26}$S$_2$) C 45.36%, H 5.11%, N 8.35%; found C 45.03%, H 4.14%, N 8.08%.
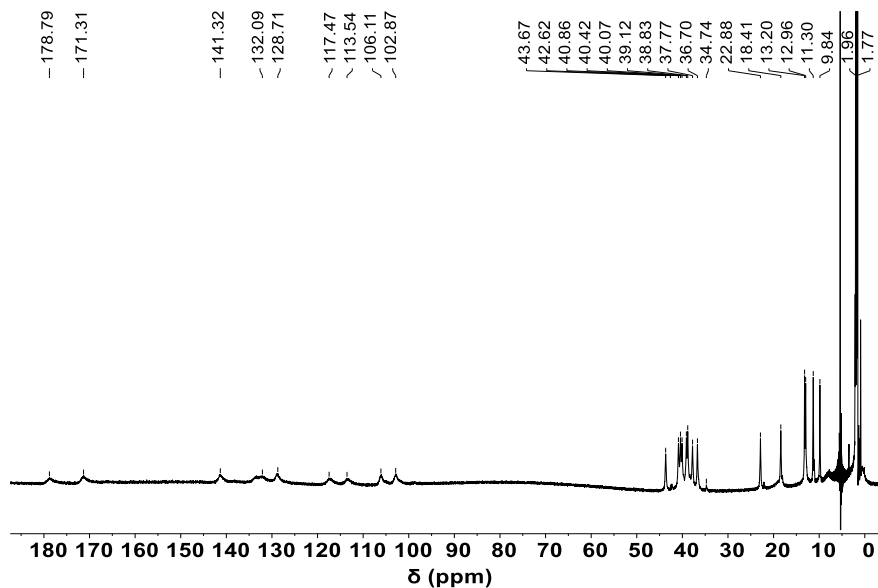
Figure S6. ^{1}H NMR spectrum of **[L$_2$Ni$_4$(CO$_3$)$_2$(H$_2$O)$_2$]$^{2+}$** (CD$_2$Cl$_2$, 25 °C, 500 MHz).
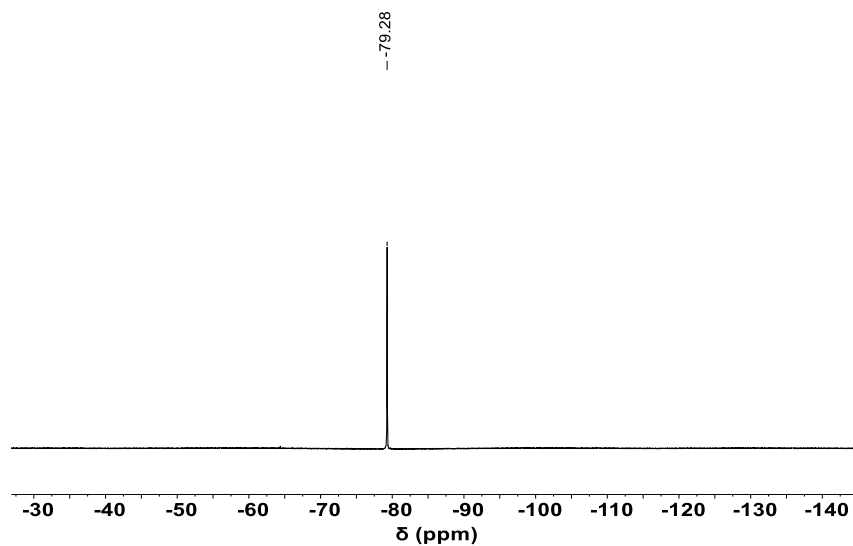
Figure S7. ^{19}F NMR spectrum of **[L$_2$Ni$_4$(CO$_3$)$_2$(H$_2$O)$_2$]$^{2+}$** (CD$_2$Cl$_2$, 25 °C, 471 MHz).
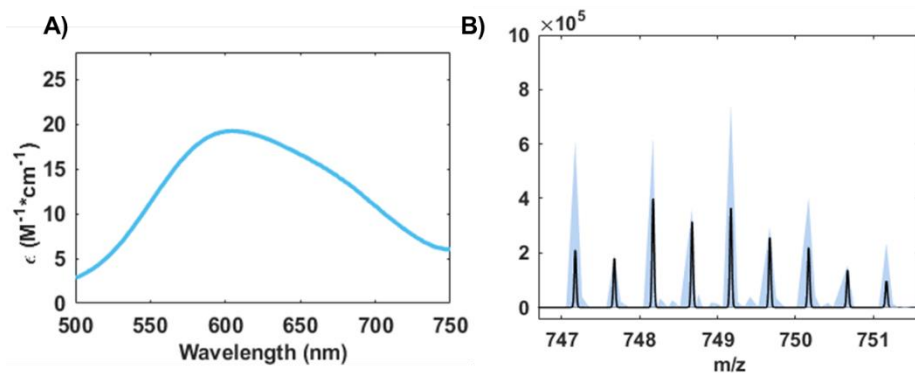
Figure S8. A) UV-visible spectrum of **[L$_2$Ni$_4$(CO$_3$)$_2$(H$_2$O)$_2$]$^{2+}$** (0.02 mM, 25 °C) in acetonitrile. **B)** Simulated (□) vs. experimental (■) ESI mass spectrum of **[L$_2$Ni$_4$(CO$_3$)$_2$(H$_2$O)$_2$]$^{2+}$**.

Synthesis of [L₂Ni₄(OH)₄][OTf]₂

[LNi₂(OTf)₂]⁺   **[L₂Ni₄(OH)₄]²⁺**
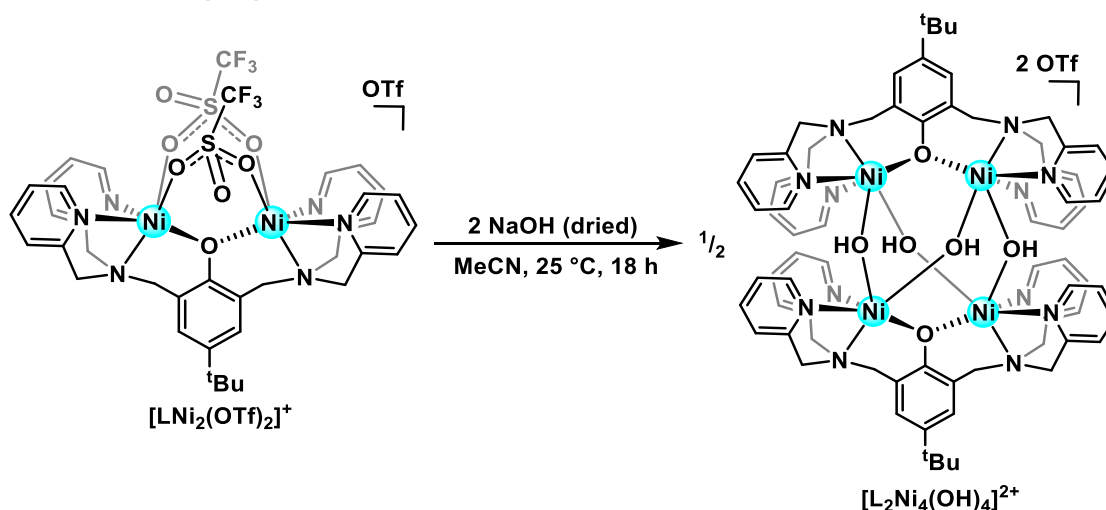
In the glovebox, a 100 mL round bottom flask was charged with **[LNi₂(OTf)₂]⁺** (750 mg, 0.66 mmol, 1 equiv.), acetonitrile (35 mL), and a magnetic stir bar. Dry NaOH (53 mg, 1.32 mmol, 2 equiv.) was added in a single portion and the reaction was left to stir for 18 hours at room temperature. The teal/blue reaction mixture was filtered through a glass frit, and the filtrate was dried under reduced pressure. Trituration with a 1:1 mixture of pentanes and diethyl ether (*ca.* 20 mL total) yielded spectroscopically pure **[L₂Ni₄(OH)₄]²⁺** as a bright blue powder (660 mg, 0.33 mmol, 98% yield [see note below on bulk compound purity]). Single pale blue crystalline plates, suitable for X-ray diffraction, were grown via vapor diffusion of pentanes into a concentrated THF solution of **[L₂Ni₄(OH)₄]²⁺** at –35 °C.

^{1}H NMR (400 MHz, CD₂Cl₂) δ (ppm): 129.31, 111.44, 100.69, 97.56, 85.01, 39.56, 38.10, 37.37, 36.26, 31.62, 20.09, 15.16, 14.35, 12.35, 10.95, 8.91.

^{19}F NMR (471 MHz, CD₂Cl₂) δ (ppm): –73.35

UV-Visible: λ (nm) 617 (ε = 49 M⁻¹cm⁻¹).

ESI MS: [L₂Ni₄(OH)₄]²⁺, calc. 723.1928; exp. 723.1913 m/z.

Elemental Analysis: Calcd. for **[L₂Ni₄(OH)₂][OTf]₂·1.66[NaOTF]** (C₇₅.₆₆H₈₂F₁₀.₉₈Na₁.₆₆N₁₂Ni₄O₁₆.₉₈S₃.₆₆) C 44.74%, H 4.07%, N 8.28%; found C 44.64%, H 4.41%, N 8.01%.

Note: Elemental analysis was conducted on powder samples obtained as described in the experimental details above. These were contaminated with a NaOTf impurity that is subsequently factored into the reported yield. The presence of outer-sphere triflate anions in the desired cluster complex convolutes determining the presence of triflate salts via ^{19}F NMR spectroscopy. We were only able to fully purify material via crystallization; however, we saw no evidence of NaOTf effecting subsequent peroxide chemistry (similar reactivity was observed from **[L₂Ni₄(CO₃)₂(H₂O)₂]²⁺** which could be rigorously purified away from salts). All preparations employing **[L₂Ni₄(OH)₂][OTf]₂·1.66[NaOTF]** assumed a molecular weight consistent with the combustion analysis results.
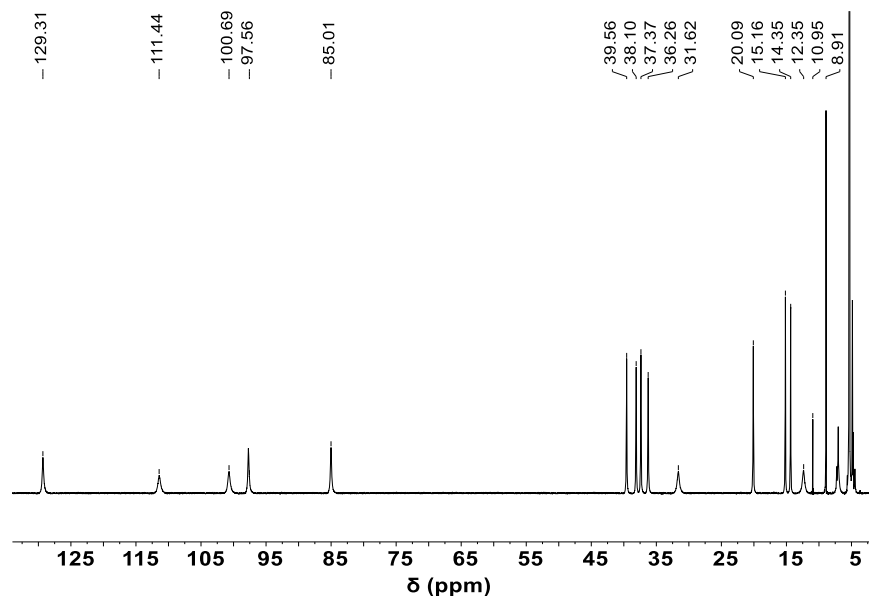
Figure S9. ^{1}H NMR of **[L$_2$Ni$_4$(OH)$_4$]$^{2+}$** (CD$_2$Cl$_2$, 25 °C, 400 MHz).
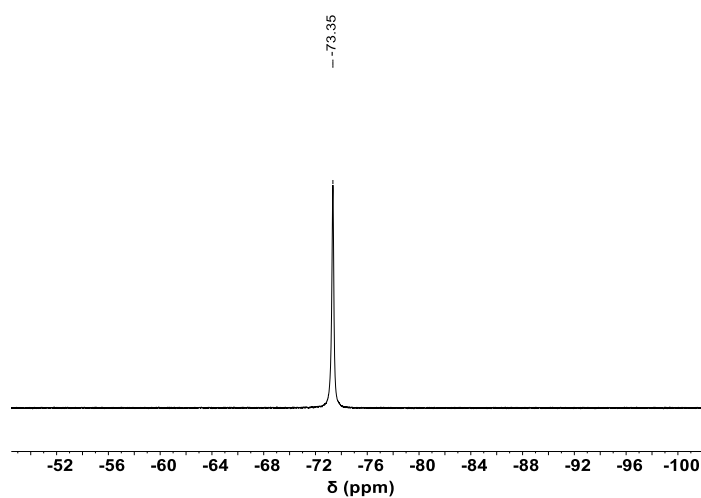
Figure S10. ^{19}F NMR of **[L$_2$Ni$_4$(OH)$_4$]$^{2+}$** (CD$_2$Cl$_2$, 25 °C, 471 MHz).
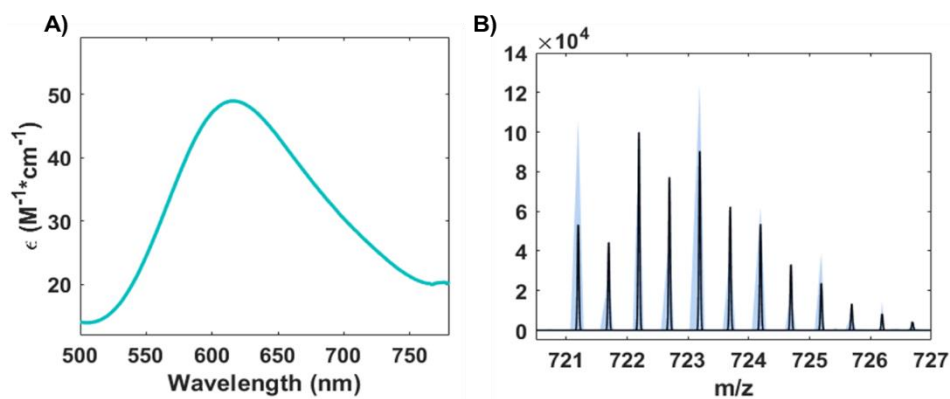
Figure S11. A) UV-visible spectrum of **[L$_2$Ni$_4$(OH)$_4$]$^{2+}$** (0.03 mM, 25 °C) in acetonitrile. **B)** Simulated (□) vs. experimental (■) ESI mass spectrum of **[L$_2$Ni$_4$(OH)$_4$]$^{2+}$**.

In-Situ Preparation of [LNi$_2$(CO$_3$H)$_2$]$^+$.
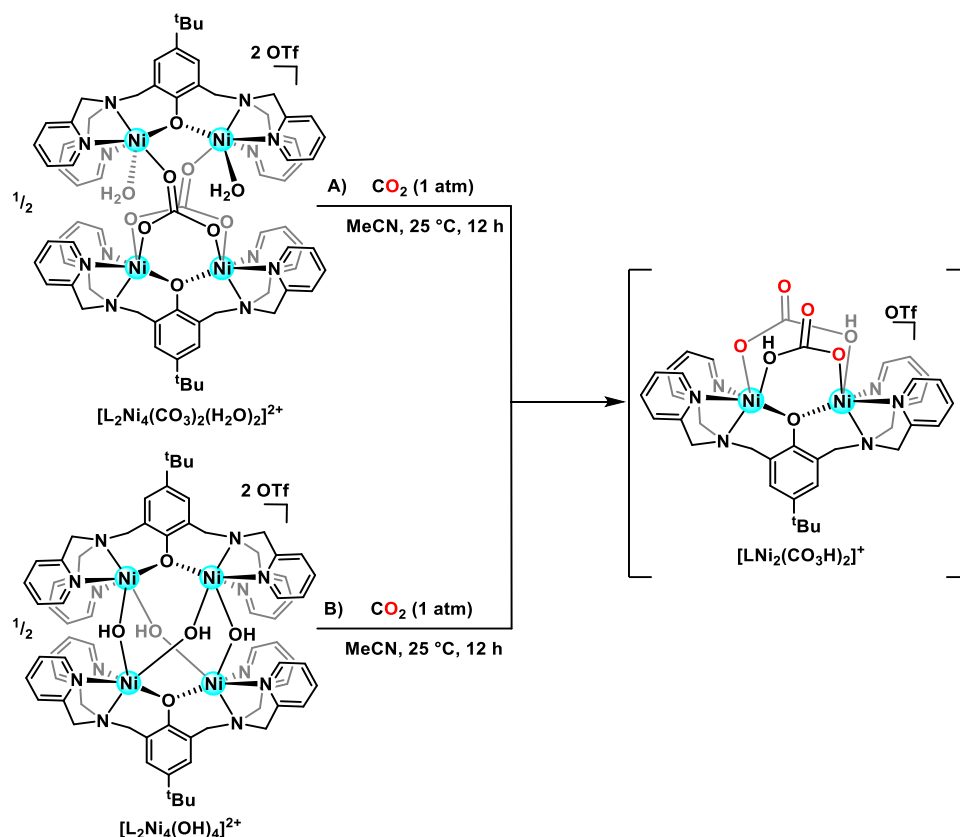
A) In the fume hood, a J. Young style NMR tube was charged with **[L$_2$Ni$_4$(CO$_3$)$_2$(H$_2$O)$_2$]$^{2+}$** (9 mg, 0.01 mmol, 1 equiv.) and CD$_3$CN (600 µL). The solution was subjected to three freeze/pump/thaw cycles, and, following the final thaw, the headspace was backfilled with CO$_2$ gas (1 atm). The NMR tube was closed and mixed via inversion for 12 hrs. ^{1}H NMR spectroscopy evidenced complete conversion to a new species, **[LNi$_2$(CO$_3$H)$_2$]$^+$**, which was used without further purification due to the propensity to dissociate CO$_2$. Repeated crystallization attempts afforded pale blue single crystals identified as **[L$_2$Ni$_4$(CO$_3$)$_2$(H$_2$O)$_2$]$^{2+}$** by ^{1}H NMR spectroscopy.

B) In the glovebox, a J. Young style NMR tube was charged with **[L$_2$Ni$_4$(OH)$_4$]$^{2+}$** (17 mg, 0.01 mmol, 1 equiv.) and CD$_3$CN (600 µL). The tube was subjected to three freeze/pump/thaw cycles, and, following the final thaw, the headspace was backfilled with CO$_2$ gas (1 atm). The NMR tube was closed and mixed via inversion for 12 hrs. ^{1}H NMR spectroscopy displayed complete conversion to **[LNi$_2$(CO$_3$H)$_2$]$^+$**, which was used without further purification.

Note: Further interrogation showed **[LNi$_2$(CO$_3$H)$_2$]$^+$** is only stable in acetonitrile solution.

^{1}H NMR (500 MHz, CH$_3$CN) δ (ppm): 136.19, 130.86, 122.65, 57.21, 43.74, 42.61, 40.33, 39.48, 22.44, 14.07, 10.36.

^{19}F NMR (471 MHz, CD$_3$CN) δ (ppm): –79.70

UV-Visible: λ (nm) 594 (ε = 10 M^{-1}cm^{-1}).

ESI MS: [LNi$_2$(CO$_3$H)$_2$]$^+$, calc. 809.1789; exp. 809.1742 m/z.
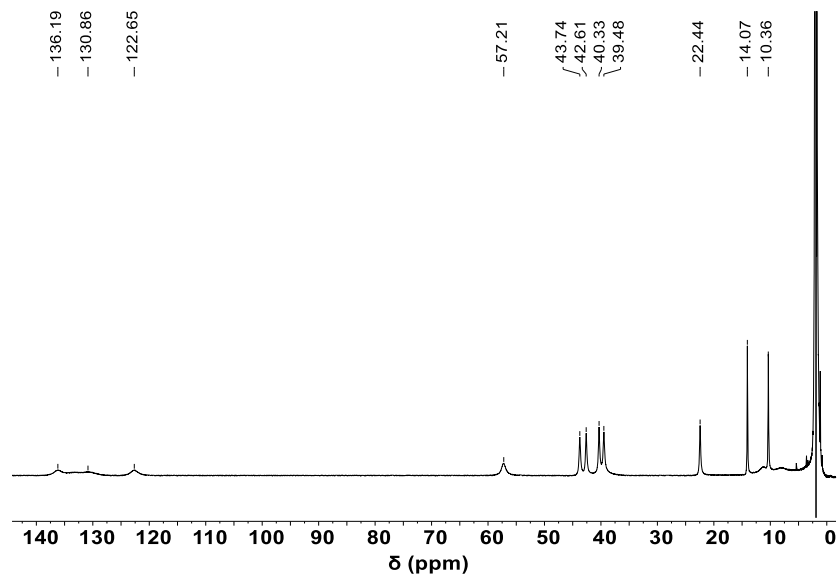
Figure S12. ^1H NMR spectrum of **[LNi$_2$(CO$_3$H)$_2$]$^+$** (CH$_3$CN, 25 °C, 500 MHz).
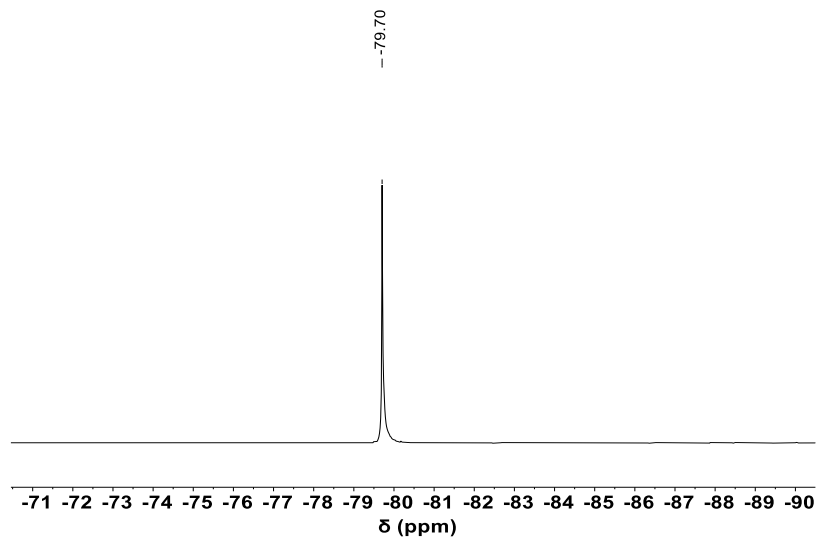
Figure S13. ^{19}F NMR spectrum of **[LNi$_2$(CO$_3$H)$_2$]$^+$** (CH$_3$CN, 25 °C, 471 MHz).
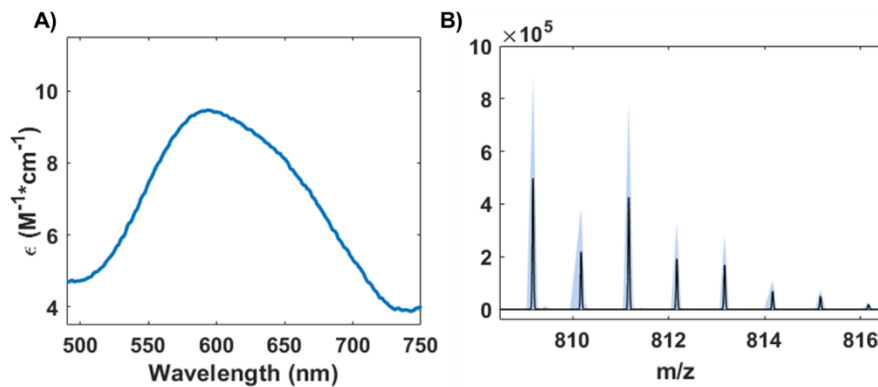
Figure S14. A) UV-visible spectrum of **[LNi$_2$(CO$_3$H)$_2$]$^+$** (0.01 mM, 25 °C) in acetonitrile. B) Simulated (□) vs. experimental (■) ESI mass spectrum of **[LNi$_2$(CO$_3$H)$_2$]$^+$**.
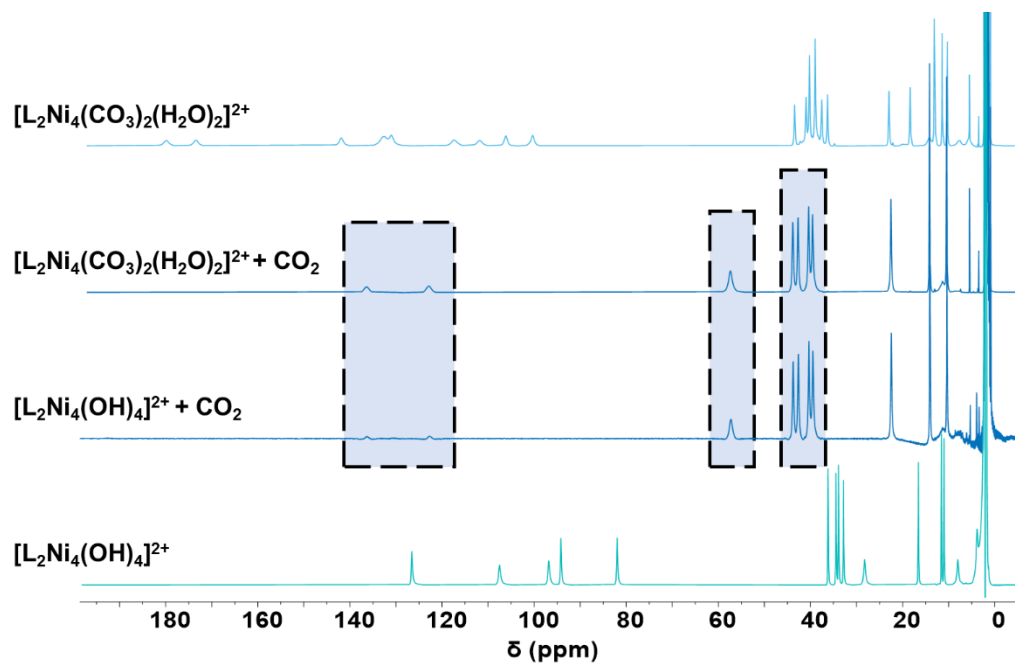
Figure S15. Stacked ^{1}H NMR spectra showing conversion of **[L$_2$Ni$_4$(CO$_3$)$_2$(H$_2$O)$_2$]$^{2+}$** (top) and **[L$_2$Ni$_4$(OH)$_4$]$^{2+}$** (bottom) to **[LNi$_2$(CO$_3$H)$_2$]$^+$** upon addition of CO$_2$ (g) (CH$_3$CN, 25 °C, 500 MHz). Blue shaded boxes (■) emphasize spectral features that distinguish the starting materials from **[LNi$_2$(CO$_3$H)$_2$]$^+$**, and show convergence to the same product.

DOSY Studies of [LNi$_2$(CO$_3$H)$_2$]$^+$ and [L$_2$Ni$_4$(OH)$_4$]$^{2+}$

To support the proposed dinuclear structure of **[LNi$_2$(CO$_3$H)$_2$]$^+$**, we pursued diffusion ordered NMR spectroscopy (DOSY) experiments.[5] As an authentic tetranuclear control complex, a CD$_3$CN (0.6 mL) solution of **[L$_2$Ni$_4$(OH)$_4$]$^{2+}$** (6 mg, 0.003 mmol) and a ferrocene standard (2 mg, 0.01 mmol) was prepared in a J. Young style NMR tube. A DOSY spectrum was collected with the following salient acquisition parameters: Doneshot pulse sequence with a spectral width of –13 to 149 ppm, an acquisition time of 0.2 seconds, a 0.1 second relaxation delay, diffusion gradient length of 2.0 milliseconds and diffusion delay of 12.0 milliseconds. An array of 10 spectra, 320 scans each, were utilized to calculate the 2D DOSY spectrum for this compound (**Figure S16**).

Note: We were unable to determine acquisition parameters that provided the same phase for the signals attributed to the paramagnetic signals of **[L$_2$Ni$_4$(OH)$_4$]$^{2+}$** and the diamagnetic signals of ferrocene. The latter is not observed in this 2D spectrum.
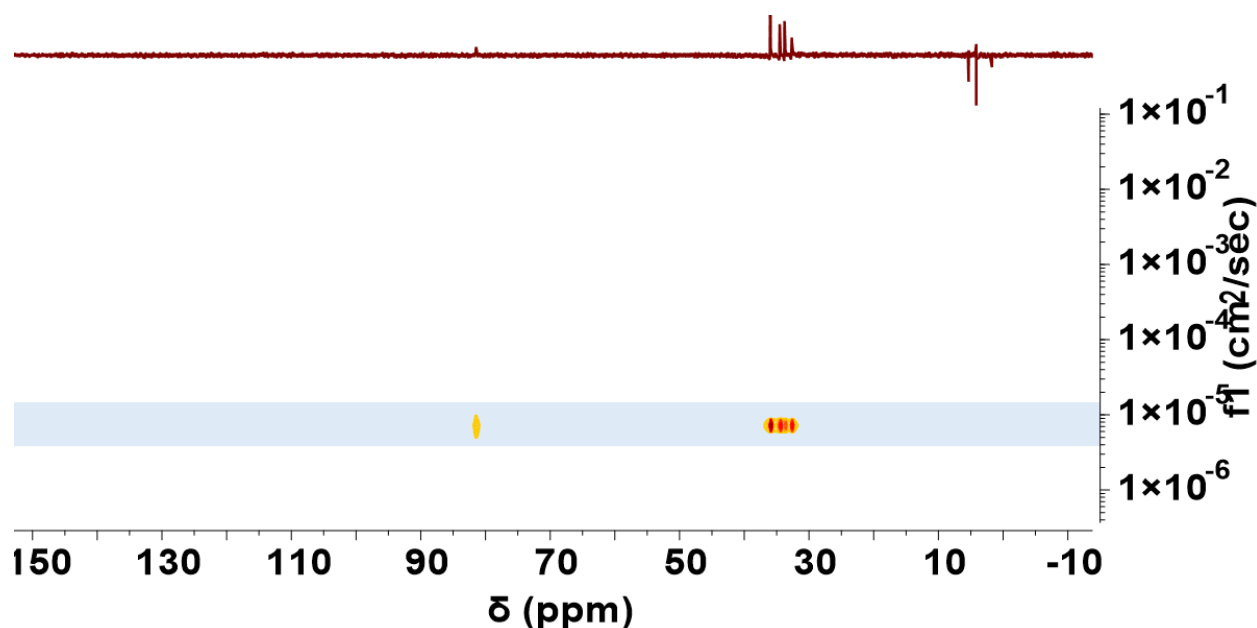
Figure S16. 2D DOSY Spectrum of **[L$_2$Ni$_4$(OH)$_4$]$^{2+}$** (^{1}H, CD$_3$CN, 25 °C, 700 MHz). The blue shadow box highlights the diffusion coefficient attributed to the tetranuclear complex.

This tube was then freeze-pump-thawed thrice and the headspace backfilled with gaseous CO$_2$ (1 atm.). After mixing by inversion for 30 minutes, a DOSY spectrum was collected with the following acquisition parameters: Doneshot pulse sequence with a spectral width of –17 to 120 ppm, an acquisition time of 0.1 seconds, a relaxation delay of 0.015 seconds, diffusion gradient length of 0.5 milliseconds and a diffusion delay of 3 milliseconds. An array of 15 spectra, each with 800 scans, were used to calculate the 2D DOSY spectrum shown (**Figure S17**).

Note: In this case, the sample and ferrocene standard signals displayed matched phasing, facilitating a direct comparison.
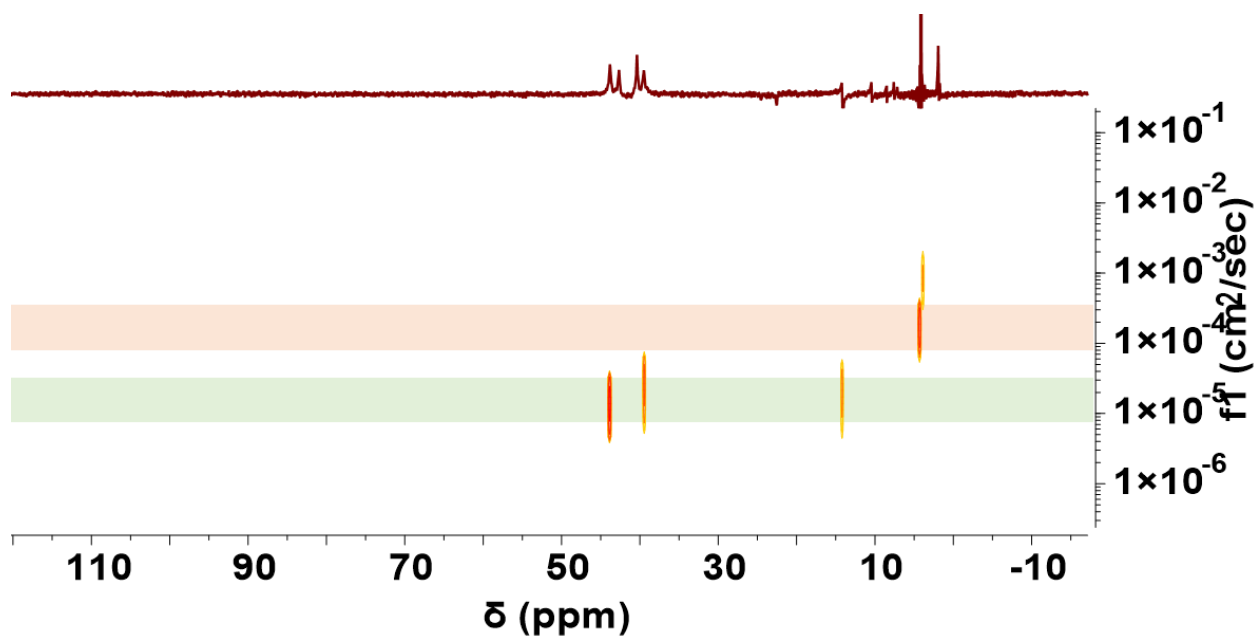
Figure S17. 2D DOSY Spectrum of **[LNi$_2$(CO$_3$H)$_2$]$^+$** (^{1}H, CD$_3$CN, 25 °C, 700 MHz). The green shadow box highlights the diffusion coefficient attributed to the dinuclear complex; the orange shadow box emphasizes the ferrocene standard signal.

Despite an inability to directly compare the diffusion coefficients for the two species, superimposing the relevant DOSY spectra (**Figure S18**) shows a diffusion coefficient for **[LNi$_2$(CO$_3$H)$_2$]$^+$** (1.83 x 10^{-5} cm^2/sec) that is roughly an order of magnitude larger than **[L$_2$Ni$_4$(OH)$_4$]$^{2+}$** (7.22 x 10^{-6} cm^2/sec), consistent with the dinuclear and tetranuclear structural assignments, respectively (for reference, ferrocene is roughly one order of magnitude bigger still: 1.23 x 10^{-4} cm^2/sec).
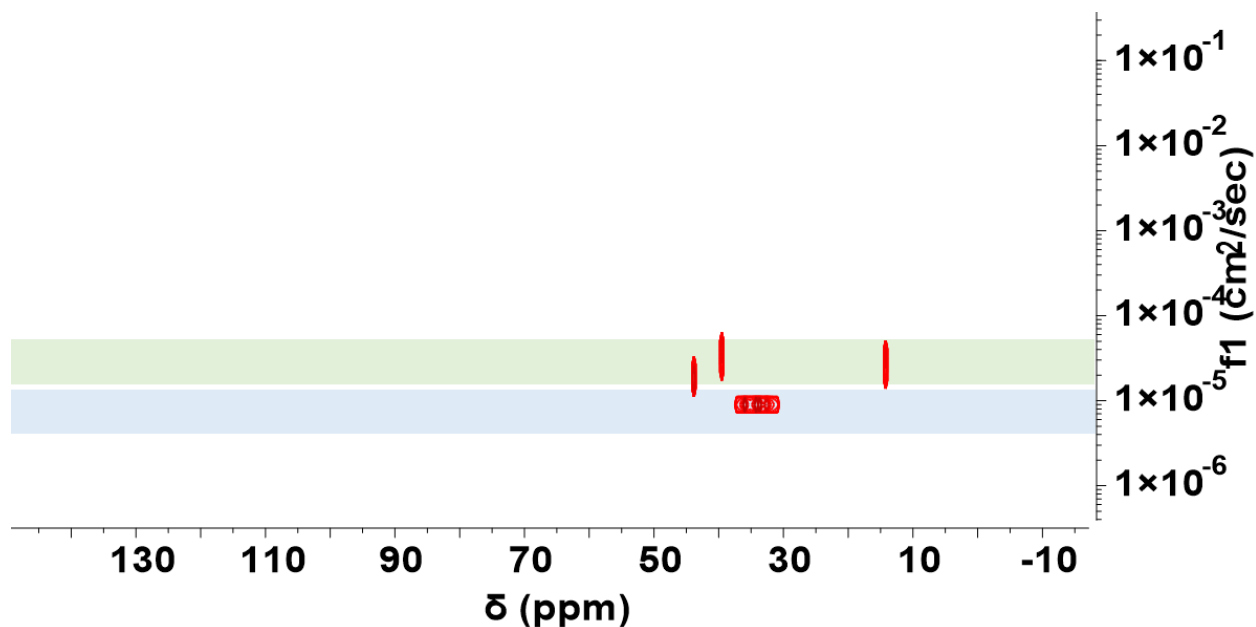
Figure S18. Superimposed 2D DOSY Spectrum of **[L$_2$Ni$_4$(OH)$_4$]$^{2+}$** and **[LNi$_2$(CO$_3$H)$_2$]$^+$** (^{1}H, CD$_3$CN, 25 °C, 700 MHz).

Synthesis of [LNi₂(O₂CO₂)(H₂O)₂][OTf]

$[L_2Ni_4(CO_3)_2(H_2O)_2]^{2+}$

A) 200 equiv. H_2O_2
excess CO_2

MeCN, −30 °C, 1 h

$[L_2Ni_4(OH)_4]^{2+}$

B) 220 equiv. H_2O_2
excess CO_2

MeCN, −30 °C, 2 h

2 $[LNi_2(O_2CO_2)(H_2O)_2]^+$
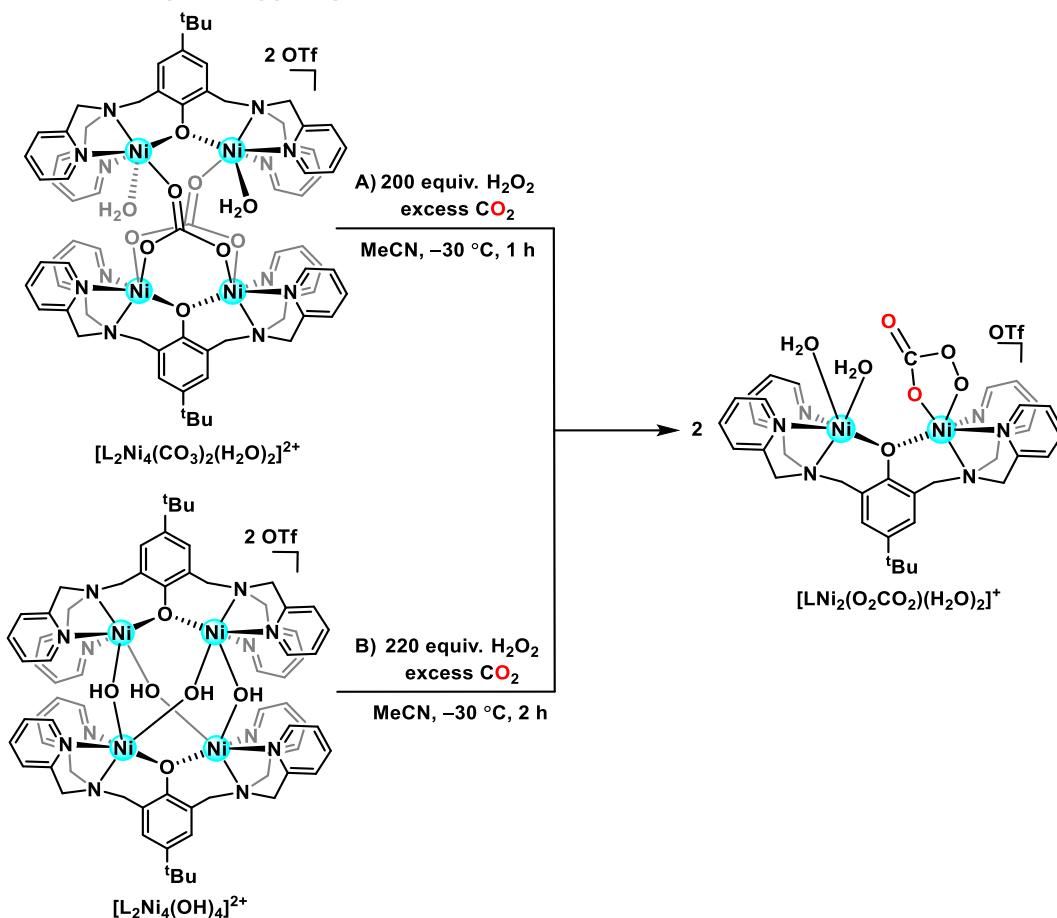
A) In a fume hood, a 20 mL scintillation vial was charged with **[L₂Ni₄(CO₃)₂(H₂O)₂]²⁺** (200 mg, 0.11 mmol, 1 equiv.), acetonitrile (10 mL), and a magnetic stir bar. The vial was placed in a dry ice/acetone bath maintained at −30 °C. Upon cooling, both H_2O_2 (50% w/w in water, 1.25 mL, 22 mmol, 200 equiv.) and a piece of dry ice (*ca.* 150 mg, 3.4 mmol, 31 equiv.) were simultaneously added to the reaction vial. The reaction was left to stir for 1 hour at −30 °C, at which time MgSO₄ was added. The mixture was filtered through a fritted glass funnel and the clear blue filtrate was concentrated to *ca.* 2 mL under reduced pressure. Diethyl ether (*ca.* 3 mL) was added, the turbid solution was filtered through Celite, and the filtrate was cooled to −17 °C in a freezer for 24 hrs. X-ray quality pale purple crystalline plates were collected and identified as **[LNi₂(O₂CO₂)(H₂O)₂]⁺** by both single-crystal XRD and ¹H NMR spectroscopy (73 mg, 0.08 mmol, 35% yield).

B) In a fume hood, **[L₂Ni₄(OH)₄]²⁺** (201 mg, 0.10 mmol, 1 equiv.) was dissolved in acetonitrile (10 mL) in a 20 mL scintillation vial charged with a stir bar. The vial was placed in a dry ice/acetone bath with temperature maintained at −30 °C. Upon cooling, both H_2O_2 (50% w/w in water, 1.5 mL, 26.5 mmol, 220 equiv.) and a piece of dry ice (*ca.* 150 mg, 3.4 mmol, 28 equiv.) were simultaneously added to the reaction vial. The reaction was left to stir for 2 hours at −30 °C, at which time MgSO₄ was added. The mixture was filtered through a sintered glass frit and the clear blue filtrate was concentrated to *ca.* 2 mL under reduced pressure. Diethyl ether (*ca.* 3 mL) was added, the turbid solution was filtered through Celite, and the filtrate was cooled to −17 °C in a freezer for 24 hours. X-ray quality pale purple crystalline plates were collected

and identified as **[LNi$_2$(O$_2$CO$_2$)(H$_2$O)$_2$]$^+$** by both single-crystal XRD and ^{1}H NMR spectroscopy (37 mg, 0.039 mmol, 20% yield).

Note: If the reaction mixture turns deep green following concentration of the acetonitrile solution, either no crystallization will occur, or the resultant product will be spectroscopically impure.

Note: This complex necessitates storage at –17 °C in crystalline form. Degradation is likely if solids are manipulated at room temperature for *ca.* 1 hour or if solutions are warmed to room temperature for any duration of time (*vide infra*).

^{1}H NMR (500 MHz, CD$_3$CN) δ (ppm): 169.71, 157.13, 130.41, 122.32, 98.37, 49.16, 47.89, 45.20, 43.75, 42.35, 41.26, 37.97, 25.91, 24.36, 21.16, 19.60, 14.02, 13.35, 12.03, 8.79, 3.41.

^{19}F NMR (564 MHz, CD$_3$CN) δ (ppm): –79.34

UV-Visible: λ (nm) 581 (ε = 6 M^{-1}cm^{-1})

ESI MS. [LNi$_2$(O$_2$CO$_2$)(H$_2$O)]$^+$: calc. 781.1773; exp. 781.1781 m/z.
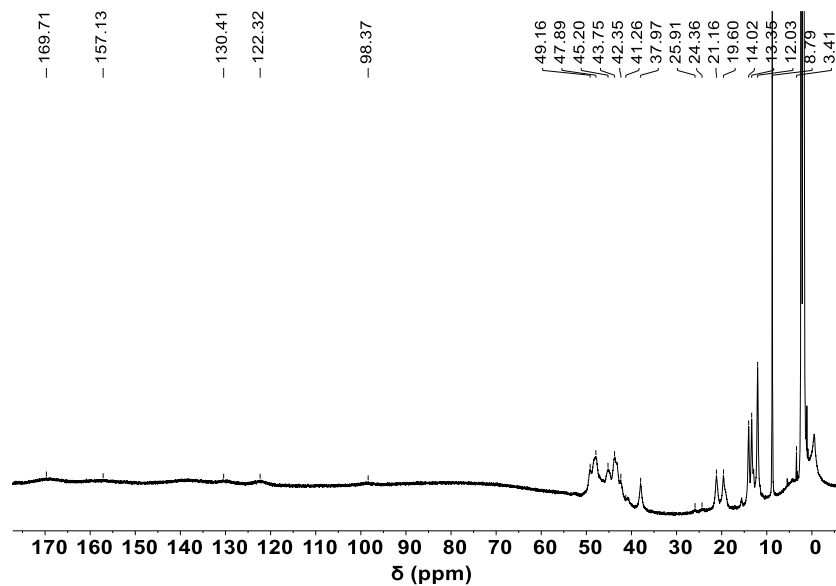
Figure S19. ^{1}H NMR spectrum of **[LNi$_2$(O$_2$CO$_2$)(H$_2$O)$_2$]$^+$** (CD$_3$CN, -25 °C, 500 MHz).
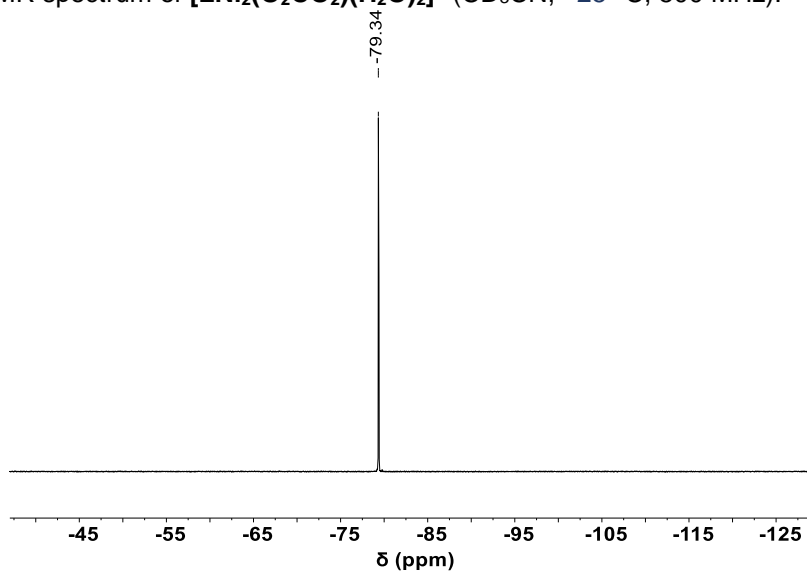
Figure S20. ^{19}F NMR spectrum of **[LNi$_2$(O$_2$CO$_2$)(H$_2$O)$_2$]$^+$** (CD$_3$CN, -25 °C, 564 MHz).
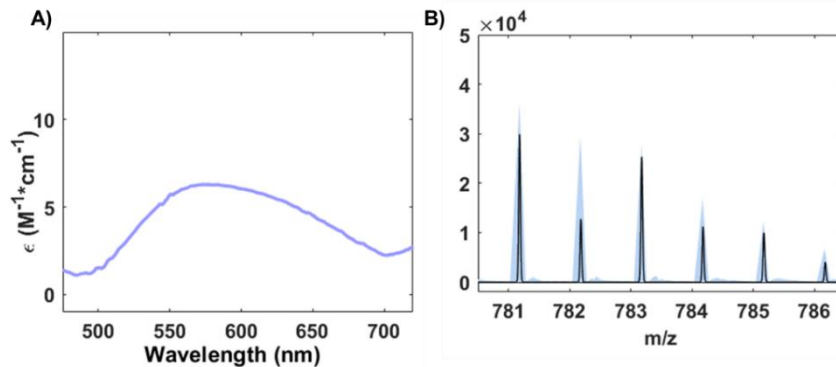
Figure S21. A) UV-visible spectrum of **[LNi$_2$(O$_2$CO$_2$)(H$_2$O)$_2$]$^+$** (0.02 mM, 25 °C) in acetonitrile. B) Simulated (□) vs. experimental (■) ESI mass spectrum of **[LNi$_2$(O$_2$CO$_2$)(H$_2$O)$_2$]$^+$**.
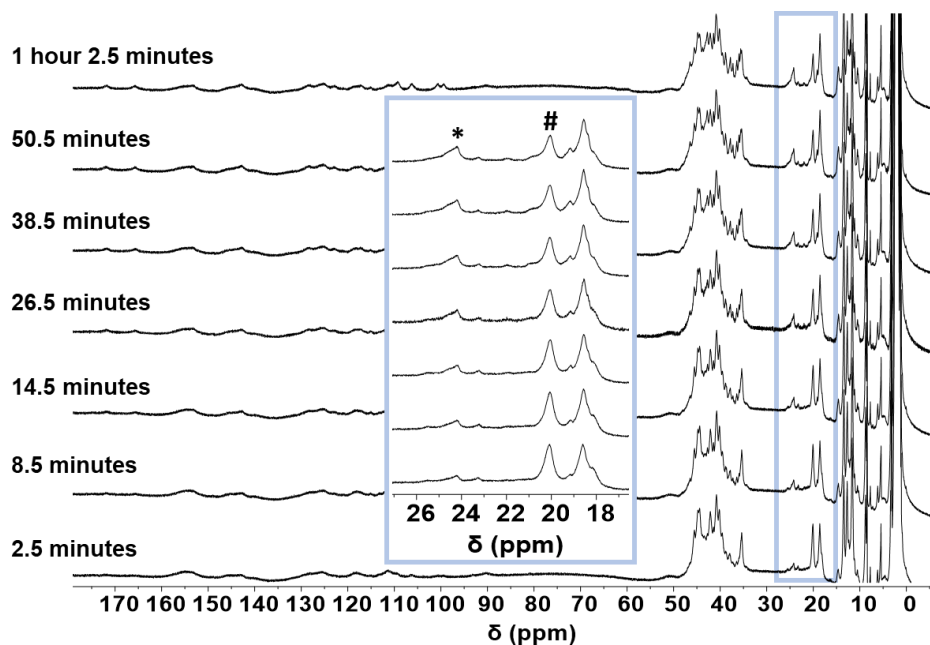
Figure S22. Low temperature ^{1}H NMR (700 MHz, 0 °C, CD$_3$CN) spectra of **[LNi$_2$(O$_2$CO$_2$)(H$_2$O)$_2$]$^+$** under N$_2$. Time points are indicated on each respective spectrum. **Boxed Inset:** Diagnostic ^{1}H NMR peaks that distinguish slow decomposition of **[LNi$_2$(O$_2$CO$_2$)(H$_2$O)$_2$]$^+$** (**#**) to **[L$_2$Ni$_4$(CO$_3$)$_2$(H$_2$O)$_2$]$^{2+}$** (*) over the course of 1 hour (*ca.* 60% conversion).
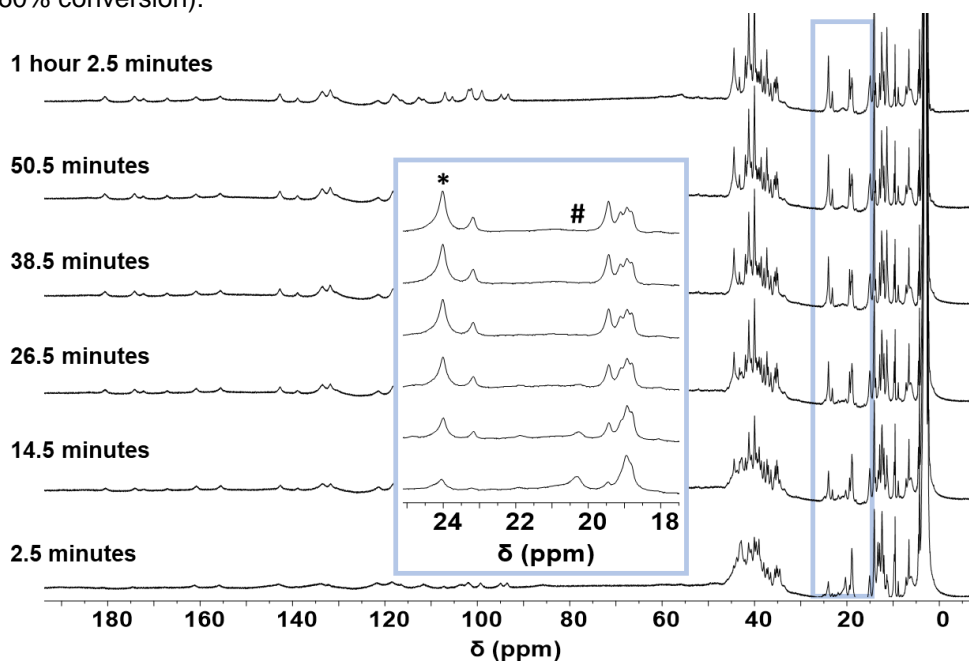
Figure S23. Time course ^{1}H NMR (700 MHz, 0 °C, CD$_3$CN) spectra of **[LNi$_2$(O$_2$CO$_2$)(H$_2$O)$_2$]$^+$** under N$_2$; time points are given for each respective spectra. Decomposition to a mixture of species is complete in less than 30 minutes at 25 °C. **Boxed Inset:** Partial ^{1}H NMR spectra that show salient peaks tracking decomposition to the tetranuclear carbonate complex and other unknown byproducts. Complete conversion of **[LNi$_2$(O$_2$CO$_2$)(H$_2$O)$_2$]$^+$** (**#**) was observed prior to the 30 minute time point. Over the course of the remaining 45 minutes, decomposition to both **[L$_2$Ni$_4$(CO$_3$)$_2$(H$_2$O)$_2$]$^{2+}$** (*) and unknown byproducts was observed.

Reactivity Studies

Indirect Quantification of H_2O_2 Released from $[LNi_2(O_2CO_2)(H_2O)_2]^+$ Upon Warming
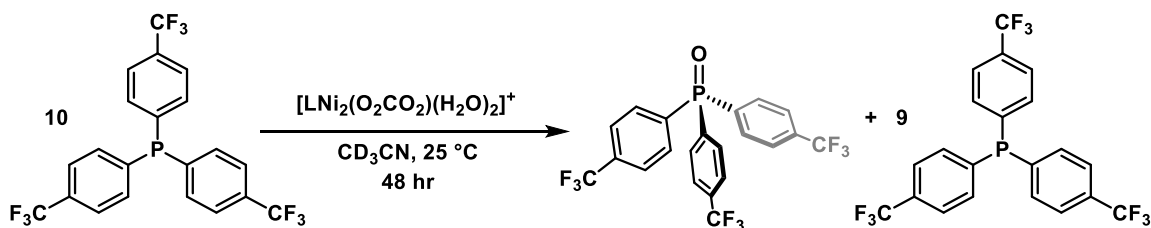
A J. Young style NMR tube was charged with **$[LNi_2(O_2CO_2)(H_2O)_2]^+$** (6 mg, 0.006 mmol, 1 equiv.) and CD_3CN (*ca.* 600 μL) was admitted via vacuum transfer. Following addition of the solvent, the headspace was backfilled with N_2 and the tube sealed. The sample was allowed to warm to room temperature and decomposition was monitored by ^1H NMR spectroscopy, as shown in **Figure S23**. Separately, tris(4-trifluoromethylphenyl)phosphine (30 mg, 0.06 mmol, 10 equiv.) and an internal standard of [bis(triphenylphosphine)iminium][BArF], [PNP][BArF], (9 mg, 0.006 mmol, 1 equiv.) were dissolved in CD_3CN (200 μL) in a dram vial. With the NMR tube under positive N_2 pressure, the tube was opened carefully, the phosphine solution was added by Hamilton syringe, and the tube was resealed. After mixing by inversion for 48 hours, the sample was taken to the NMR spectrometer and a $^{31}P\{^1H\}$ NMR spectrum was collected at 25 °C to quantify the unreacted tris(4-trifluoromethylphenyl)phosphine and its oxidized form (0.006 mmol, 92% yield), the latter serving as a reporter for the amount of H_2O_2 released from the decomposition of **$[LNi_2(O_2CO_2)(H_2O)_2]^+$**.

Note: The room temperature conversion of **$[LNi_2(O_2{}^{13}CO_2)(H_2O)_2]^+$** to **$[L_2Ni_4({}^{13}CO_3)_2(H_2O)_2]^{2+}$** shows a small but detectable amount of $^{13}CO_2$ is released as verified by $^{13}C\{^1H\}$ NMR spectroscopy (*viz.* **Figure S34**). This result is consistent with the conversion of **$[LNi_2(O_2CO_2)(H_2O)_2]^+$** to **$[L_2Ni_4(CO_3)_2(H_2O)_2]^{2+}$** being high yielding but not quantitative.
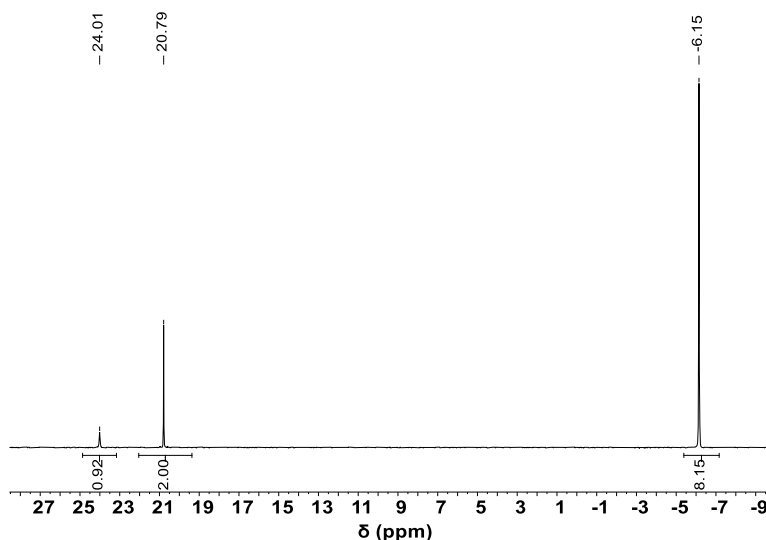
Figure S24. $^{31}P\{^1H\}$ NMR (283 MHz, 25 °C, CD_3CN) spectrum of excess tris(4-trifluoromethylphenyl) phosphine addition to a mixture of **$[L_2Ni_4(CO_3)_2(H_2O)_2]^{2+}$** and H_2O_2 generated via thermal degradation of **$[LNi_2(O_2CO_2)(H_2O)_2]^+$**. Both the tris(4-trifluoromethylphenyl)phosphine (–6.15 ppm) and phosphine oxide (24.01 ppm) peaks are integrated relative to a [PNP][BArF] internal standard (20.79 ppm).

Tris(4-trifluoromethylphenyl)phosphine Oxidation Control

A J. Young style NMR tube was charged with tris(4-trifluoromethylphenyl)phosphine (39 mg, 0.08 mmol, 10 equiv.), [PNP][BArF] (12 mg, 0.008 mmol, 1 equiv.), and CD_3CN (500 µL) under air. The NMR probe was precooled to 0 °C, and an initial $^{31}P\{^1H\}$ NMR spectrum was collected to quantify the amount of phosphine oxide impurity present in as-received commercial tris(4-trifluoromethylphenyl) phosphine (0.008 mmol, *ca.* 9%). The NMR tube was then removed from the spectrometer and poured into a 20 mL scintillation vial charged with **[L₂Ni₄(CO₃)₂(H₂O)₂]²⁺** (15 mg, 0.008 mmol, 1 equiv.) pre-cooled to 0 °C in an ice bath. The blue solution was then transferred back to the J. Young style NMR tube and an initial spectrum was collected at 0 °C (to match the conditions employed for phosphine oxidation reactions with **[LNi₂(O₂CO₂)(H₂O)₂]⁺**), reflecting no increase in the amount of phosphine oxide present (0.008 mmol, *ca.* 9%; **Figure S25A)**. The reaction mixture was then allowed to warm to room temperature and was mixed by inversion for 1 hour. A second $^{31}P\{^1H\}$ NMR measurement was obtained at room temperature showing no significant change to the amount of phosphine oxide present (0.008 mmol, *ca.* 10%; **Figure S25B**). Finally, the tube was subjected to three freeze/pump/thaw cycles, and the headspace backfilled with 1 atm of O_2. Subsequent inversion mixing at room temperature for 2 days did not result in further phosphine oxide generation, as confirmed by $^{31}P\{^1H\}$ NMR spectroscopy (0.008 mmol, *ca.* 10%; **Figure S25C**).
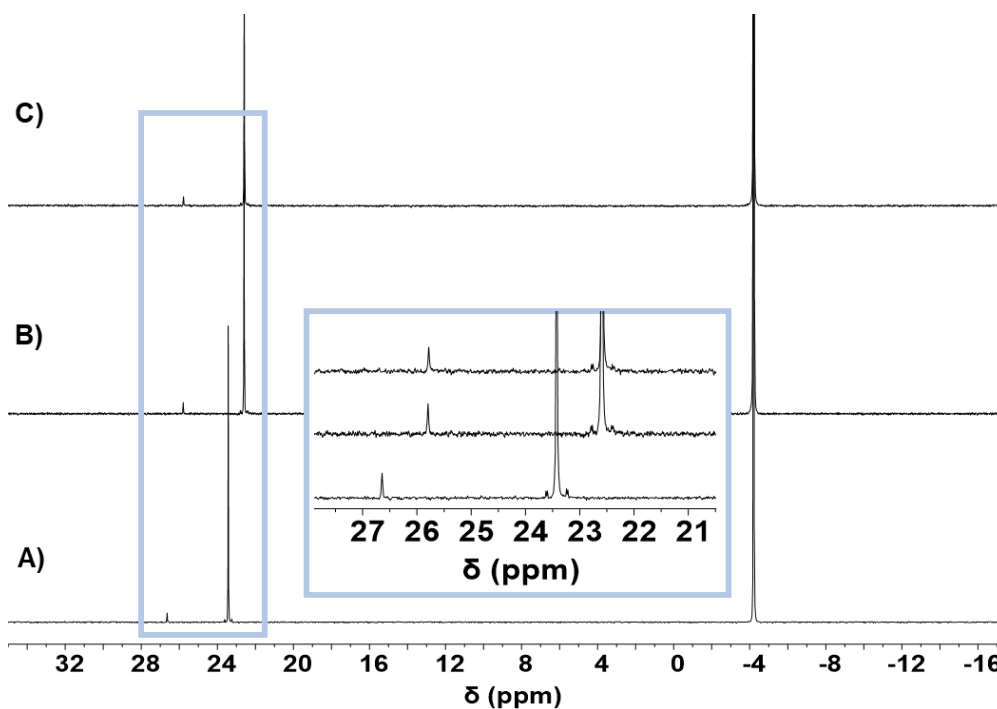
Figure S25. $^{31}P\{^1H\}$ NMR (283 MHz, 25 °C, CD_3CN) spectra of tris(4-trifluoromethylphenyl) phosphine oxidation control reactions: **A)** commercial phosphine, standard, and **[L₂Ni₄(CO₃)₂(H₂O)₂]²⁺** under air at 0 °C, **B)** the same reaction mixture after 1 hour at 25 °C, and **C)** further addition of 1 atm O_2 at 25 °C for 2 days.

Note: The shift in $^{31}P\{^1H\}$ signals in spectrum **(A)** is due to the low temperature collection of that data set (0 °C). Collecting a spectrum of commercial phosphine and standard in CD_3CN at room temperature (25 °C) affords the same chemical shifts as seen in **(B)** and **(C)**.

H₂O₂ addition to [LNi₂(O₂CO₂)(H₂O)₂]⁺

A J. Young style NMR tube was charged with **[LNi₂(O₂CO₂)(H₂O)₂]⁺** (5 mg, 0.005 mmol, 1 equiv.) and cooled in a dry ice/acetone bath. The tube was evacuated under reduced pressure, and CD₃CN (500 µL) was admitted via vacuum transfer from a calibrated volume flask. Following this addition, the tube was backfilled with N₂ and, with an active N₂ flow, a Hamilton syringe was used to slowly add a stock solution of H₂O₂ in MeCN (50 µL addition, 0.9 µL H₂O₂, 0.005 mmol, 1 equiv.) and the tube was sealed. After waiting 5 minutes for the added reagents to freeze, the tube was quickly evacuated, and the headspace refilled with N₂. This process was repeated twice to remove any trace atmosphere admitted during the syringe addition, and the tube was sealed with 1 atm of N₂ in the headspace after the third cycle. The sample was thawed immediately prior to introduction to an NMR probe pre-cooled to 0 °C. ¹H NMR spectra were obtained over 18 minutes at 0 °C (512 scans, 4 total spectra).
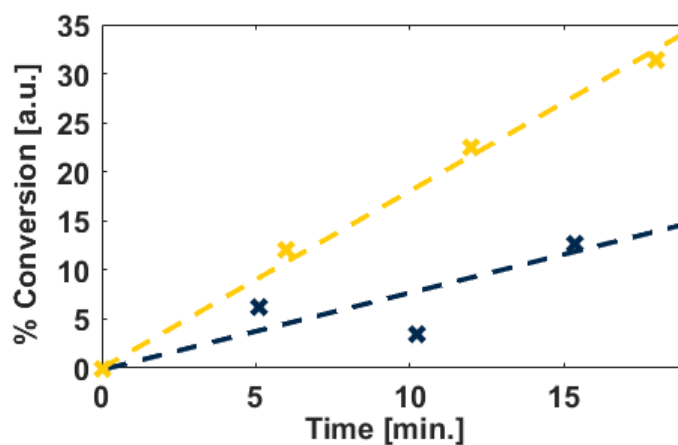
Figure S26. Comparative **[LNi₂(O₂CO₂)(H₂O)₂]⁺** decomposition kinetics at 0 °C under N₂ in the presence (x) and absence of (x) 1 equiv. H₂O₂.

Tris(4-trifluoromethylphenyl)phosphine Oxidation under N$_2$

A J. Young style NMR tube was charged with **[LNi$_2$(O$_2$CO$_2$)(H$_2$O)$_2$]$^+$** (8 mg, 0.008 mmol, 1 equiv.), tris(4-trifluoromethylphenyl)phosphine (40 mg, 0.09 mmol, 10 equiv.) and [PNP][BArF] (13 mg, 0.009 mmol, 1 equiv.) as solids. The tube was cooled in a dry ice/acetone bath and evacuated under reduced pressure. Keeping the J. Young tube in the cooling bath, CD$_3$CN (500 µL) was admitted via vacuum transfer from a calibrated volume flask. The tube was then backfilled with *ca.* 1 atm N$_2$ and resealed. The reaction mixture was mixed immediately upon thawing and carefully transferred to an NMR probe precooled to 0 °C. ^{31}P{^{1}H} NMR spectra were obtained over 20 minutes (each measurement spanned 64 seconds with 32 scans, 20 total spectra). The [PNP][BArF] standard was used to quantify unreacted phosphine and phosphine oxide at each time point via relative integration; the percent conversion vs. time was plotted, representing the reaction rate (**Figure S27**).

Note: The data presented reflects the average of duplicate kinetics assays. Each experiment utilized an independently prepared batch of **[LNi$_2$(O$_2$CO$_2$)(H$_2$O)$_2$]$^+$** to ensure sample integrity.
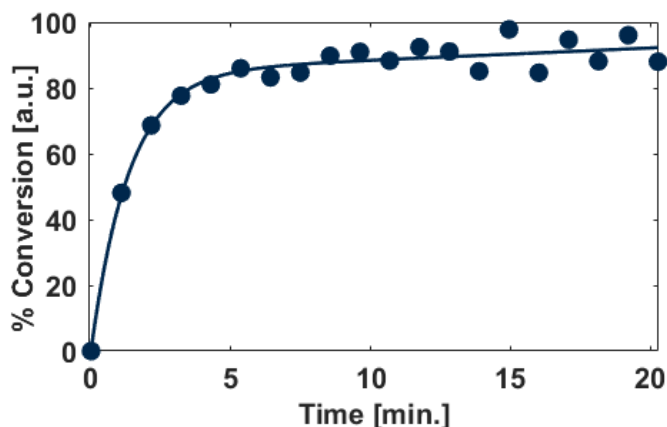
Figure S27. Time course for **[LNi$_2$(O$_2$CO$_2$)(H$_2$O)$_2$]$^+$** reactivity with tris(4-trifluoromethylphenyl) phosphine under 1 atm of N$_2$ at 0 °C.

Triphenylphosphine Oxidation under N_2

A J. Young style NMR tube was charged with **[LNi$_2$(O$_2$CO$_2$)(H$_2$O)$_2$]$^+$** (8 mg, 0.008 mmol, 1 equiv.) and placed in a dry ice/acetone bath before slowly adding CD$_3$CN (350 µL) via Hamilton syringe. After the CD$_3$CN had frozen, the NMR tube was evacuated under reduced pressure and subjected to two, freeze/pump/thaw cycles (taking care not to allow the solution to warm much beyond thawing). The sample was again frozen, and with a heavy N_2 counter flow THF stock solutions (100 µL each) of PPh$_3$ (11 mg, 0.04 mmol, 5 equiv.) and [PNP][BArF] (12 mg, 0.009 mmol, 1 equiv.) were added via syringe. The contents of the tube were mixed immediately upon thawing and carefully transferred to an NMR probe precooled to 0 °C. ^{31}P{^{1}H} NMR spectra were obtained over 20 minutes at 0 °C (each measurement spanned approximately 145 seconds with 64 scans, 8 total spectra). The [PNP][BArF] standard was used to quantify unreacted phosphine and phosphine oxide at each time point via relative integration; the percent conversion vs. time was plotted, representing the reaction rate (**Figure S28**).

Note: Mixed solvent was required due to limited solubility of PPh$_3$ in CD$_3$CN at low temperature.

Note: The data presented reflects the average of duplicate kinetics assays. Each experiment utilized an independently prepared batch of **[LNi$_2$(O$_2$CO$_2$)(H$_2$O)$_2$]$^+$** to ensure sample integrity.
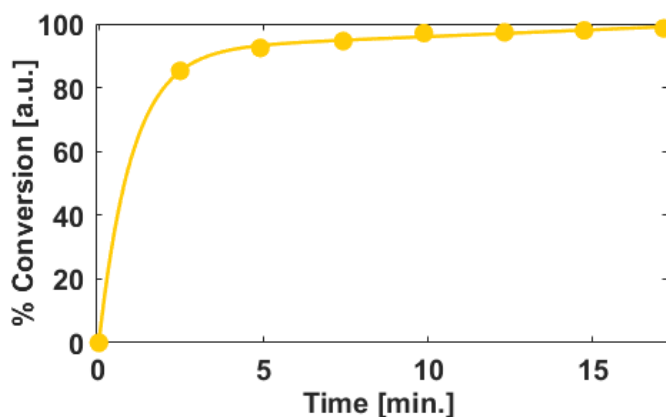
Figure S28. Time course for **[LNi$_2$(O$_2$CO$_2$)(H$_2$O)$_2$]$^+$** reactivity with PPh$_3$ under 1 atm of N_2 at 0 °C.

Tris(4-trifluoromethylphenyl)phosphine Oxidation under CO$_2$.

A J. Young style NMR tube was charged with **[LNi$_2$(O$_2$CO$_2$)(H$_2$O)$_2$]$^+$** (8 mg, 0.008 mmol, 1 equiv.), tris(4-trifluoromethylphenyl)phosphine (40 mg, 0.09 mmol, 10 equiv.) and [PNP][BArF] (13 mg, 0.009 mmol, 1 equiv.) as solids. The tube was cooled in a dry ice/acetone bath and evacuated under reduced pressure. Keeping the J. Young tube in the cooling bath, CD$_3$CN (500 µL) was admitted via vacuum transfer from a calibrated volume. The tube was then backfilled with *ca.* 1 atm N$_2$ and resealed. The reaction mixture was mixed immediately upon thawing and carefully transferred to an NMR probe precooled to 0 °C. ^{31}P{^{1}H} NMR spectra were obtained over 20 minutes at 0 °C (each measurement spanned 64 seconds with 32 scans, 20 total spectra). The [PNP][BArF] standard was used to quantify unreacted phosphine and phosphine oxide at each time point via relative integration; the percent conversion vs. time was plotted, representing the reaction rate (**Figure S29**).

Note: The data presented reflects the average of duplicate kinetics assays. Each experiment utilized an independently prepared batch of **[LNi$_2$(O$_2$CO$_2$)(H$_2$O)$_2$]$^+$** to ensure sample integrity.
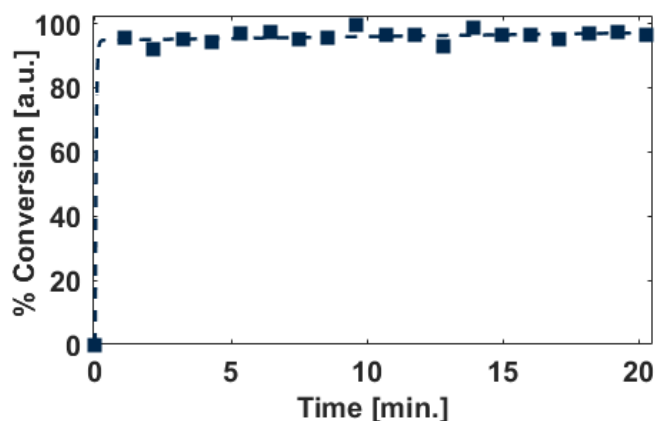
Figure S29. Time course for **[LNi$_2$(O$_2$CO$_2$)(H$_2$O)$_2$]$^+$** reactivity with tris(4-trifluoromethylphenyl) phosphine under 1 atm of CO$_2$ at 0 °C.

9,10-Dihyrdoanthracene Oxidation

10 — 9,10-dihydroanthracene $\xrightarrow[\text{4 hr}]{\substack{\text{H}_2\text{O}_2 \text{ or } [\text{LNi}_2(\text{O}_2\text{CO}_2)(\text{H}_2\text{O})_2]^+ \\ \text{DCM/MeCN, 0 °C}}}$ **No reaction**
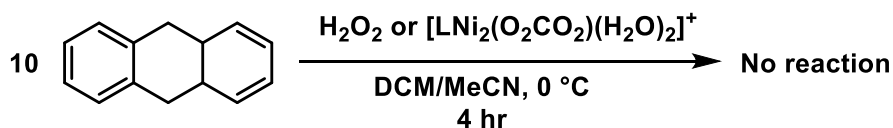
H₂O₂ Control

In a fume hood, a 20 mL scintillation vial was charged with a DCM stock solution of 9,10-dihydroanthracene (250 µL, 0.22 M, 0.055 mmol) and a magnetic stir bar. Acetonitrile (650 µL) was added to achieve a total volume of 900 µL. After stirring for 5 minutes at room temperature, an aliquot (300 µL) was filtered through a short silica plug (*ca.* 0.25") in a 9" Pasteur pipette into an NMR tube. The silica plug was rinsed with 200 µL of CD_3CN and the filtrate was likewise added to the NMR tube. A stock solution of 1,3,5-trimethoxybenzene (100 µL, 0.055 M, 0.006 mmol) was added as an internal standard. An initial (T_0) NMR spectrum was collected, and starting material was quantified by relative integration against the internal standard.

The scintillation vial with the remaining reaction solution (600 µL) was then placed in an ice water bath maintained at 0 °C. An acetonitrile stock solution of 50 wt% aqueous H_2O_2 (100 µL, 0.04 M, 0.004 mmol [Note: the amount of H_2O_2 added was adjusted to account for the substrate removed for the T_0 time point]) was added and the reaction was stirred vigorously for 4 hours at 0 °C. At this time, an aliquot (300 µL) was removed and filtered through a short silica plug (*ca.* 0.25") in a 9" Pasteur pipette. The silica plug was rinsed with 200 µL of CD_3CN and the combined filtrates transferred to an NMR tube. A 1,3,5-trimethoxybenzene standard solution (100 µL, 0.055 M, 0.006 mmol) was added. Starting material conversion was quantified by integration of the ^{1}H NMR spectrum. Good mass balance (>95%) was observed for duplicate runs; no oxidation products were detected.

Run 1: 2.7% conversion
Run 2: 2.2% conversion   **Average: 3% conversion**

[LNi₂(O₂CO₂)(H₂O)₂]⁺ Oxidation

The same procedure outlined above was repeated, except an MeCN stock solution of **[LNi₂(O₂CO₂)(H₂O)₂]⁺** (100 µL, 0.04 M, 0.004 mmol, 1 equiv.) was added as the oxidant in lieu of the H_2O_2 stock solution. Both a T_0 aliquot and 4-hour aliquot were analyzed to quantify starting material conversion. Good mass balance (>95%) was observed for duplicate runs; no oxidation products were detected.

Run 1: 1.6% conversion
Run 2: 4.4% conversion   **Average: 3% conversion**

The lack of observed reactivity between 9,10-DHA and **[LNi₂(O₂CO₂)(H₂O)₂]⁺** suggests that that latter is not competent for the activation of weak C–H bonds. This contrasts the reactivity observed for a related monometallic iron peroxycarbonate.[6] H_2O_2 likewise does not react with 9,10-DHA under the reaction conditions.

Cis-cyclooctene Oxidation
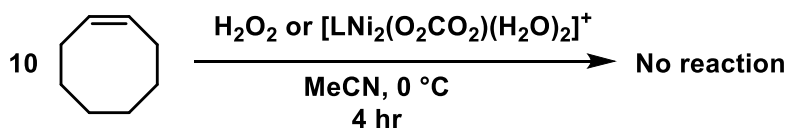
$$10 \quad \text{(cyclooctene)} \xrightarrow[\substack{\text{MeCN, 0 °C} \\ \text{4 hr}}]{\text{H}_2\text{O}_2 \text{ or } [\text{LNi}_2(\text{O}_2\text{CO}_2)(\text{H}_2\text{O})_2]^+} \text{No reaction}$$

H_2O_2 Control

In a fume hood, a 20 mL scintillation vial was charged with a MeCN stock solution of *cis*-cyclooctene (100 µL, 0.55 M, 0.055 mmol) and a magnetic stir bar. Acetonitrile (800 µL) was added to achieve a total volume of 900 µL. After stirring for 5 minutes at room temperature, an aliquot (300 µL) was filtered through a short silica plug (*ca.* 0.25") in a 9" Pasteur pipette into an NMR tube. The silica plug was rinsed with 200 µL of CD_3CN and the filtrate likewise added to the NMR tube. A stock solution of 1,3,5-trimethoxybenzene (100 µL, 0.055 M, 0.006 mmol) was added as an internal standard. An initial (T_0) NMR spectrum was collected, and starting material was quantified by relative integration against the internal standard.

The scintillation vial with the remaining reaction solution (600 µL) was then placed in an ice water bath maintained at 0 °C. An acetonitrile stock solution of 50 wt% aqueous H_2O_2 (100 µL, 0.04 M, 0.004 mmol [Note: the amount of H_2O_2 was adjusted to account for the substrate removed for the T_0 time point]) was added and the reaction was stirred vigorously for 4 hours at 0 °C. At this time, an aliquot (300 µL) was removed and filtered through a short silica plug (*ca.* 0.25") in a 9" Pasteur pipette. The silica plug was rinsed with 200 µL of CD_3CN and the combined filtrates transferred to an NMR tube. A 1,3,5-trimethoxybenzene standard solution (100 µL, 0.055 M, 0.006 mmol) was added. Starting material conversion was quantified by integration of the ^1H NMR spectrum. Acceptable mass balance (>90%) was observed for duplicate runs; no oxidation products were detected.

Run 1: 5.9% conversion
Run 2: 6.2% conversion   **Average: 6% conversion**

[LNi₂(O₂CO₂)(H₂O)₂]⁺ Oxidation

The same procedure outlined above was repeated, except an MeCN stock solution of **[LNi₂(O₂CO₂)(H₂O)₂]⁺** (100 µL, 0.04 M, 0.004 mmol, 1 equiv.) was added as the oxidant in lieu of the H_2O_2 stock solution. Both a T_0 aliquot and 4-hour aliquot were analyzed to quantify starting material conversion and product formation. Acceptable mass balance (>90%) was observed for duplicate runs; no oxidation products were detected.

Run 1: 6.1% conversion
Run 2: 7.8% conversion   **Average: 7% conversion**

Cyclooctene was investigated as a substrate given its established oxidation reactivity with one of Suzuki's iron peroxycarbonate complexes.[6] For iron, cyclooctene was oxidized to mixtures predominantly comprised of the *cis*-diol and epoxide. In contrast, no reaction is observed between **[LNi₂(O₂CO₂)(H₂O)₂]⁺** and *cis*-cyclooctene. H_2O_2 likewise shows no conversion under the reaction conditions.

4-methoxythioanisole Oxidation
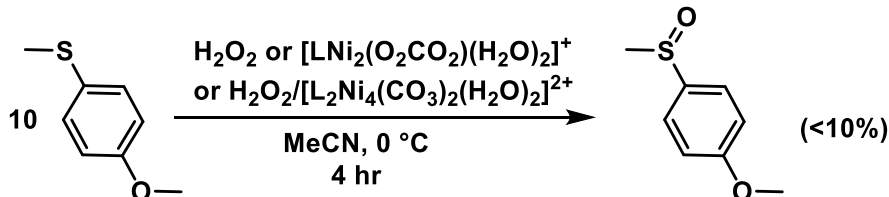
H$_2$O$_2$ Control

In a fume hood, a 20 mL scintillation vial was charged with a MeCN stock solution of 4-methoxythioanisole (250 µL, 0.22 M, 0.055 mmol) and a magnetic stir bar. Acetonitrile (650 µL) was added to achieve a total volume of 900 µL. After stirring for 5 minutes at room temperature, an aliquot (300 µL) was filtered through a short silica plug (*ca.* 0.25") in a 9" Pasteur pipette into an NMR tube. The silica plug was rinsed with 200 µL of CD$_3$CN and the filtrate likewise added to the NMR tube. A stock solution of 1,3,5-trimethoxybenzene (100 µL, 0.055 M, 0.006 mmol) was added as an internal standard. An initial (T$_0$) NMR spectrum was collected, and starting material was quantified by relative integration against the internal standard.

The scintillation vial with the remaining reaction solution (600 µL) was then placed in an ice water bath maintained at 0 °C. An acetonitrile stock solution of 50 wt% aqueous H$_2$O$_2$ (100 µL, 0.04 M, 0.004 mmol [Note: the amount of H$_2$O$_2$ was adjusted to account for the substrate removed for the T$_0$ time point]) was added and the reaction was stirred vigorously for 4 hours at 0 °C. At this time, an aliquot (300 µL) was removed and filtered through a short silica plug (*ca.* 0.25") in a 9" Pasteur pipette. The silica plug was rinsed with 200 µL of CD$_3$CN and the combined filtrates transferred to an NMR tube. A 1,3,5-trimethoxybenzene standard solution (100 µL, 0.055 M, 0.006 mmol) was added. Starting material conversion was quantified by integration of the ^{1}H NMR spectrum. Acceptable mass balance (>90%) was observed for duplicate runs; no oxidation products were detected.

Run 1: 7.5% conversion
Run 2: 8.9% conversion   **Average: 8% conversion**

[LNi$_2$(O$_2$CO$_2$)(H$_2$O)$_2$]$^+$ Oxidation

The same procedure outlined above was repeated, except an MeCN stock solution of **[LNi$_2$(O$_2$CO$_2$)(H$_2$O)$_2$]$^+$** (100 µL, 0.04 M, 0.004 mmol, 1 equiv.) was added as the oxidant in lieu of the H$_2$O$_2$ stock solution. Both a T$_0$ aliquot and 4-hour aliquot were analyzed to quantify starting material conversion and product formation. Trace oxidation product (sulfoxide) was detected.

Run 1: 11.6% conversion / 0.84% product formation (8.4% relative to H$_2$O$_2$)
Run 2: 17.0% conversion / 1.0% product formation (10.0% relative to H$_2$O$_2$)

Average: 14% conversion / 0.9% product formation
(9% relative to H$_2$O$_2$)

Literature reports show that 4-methoxyanisole will undergo oxidation by H_2O_2 in the presence of a Lewis acid catalyst.[7] In an attempt to control for reactivity mediated by nickel Lewis acids other than the peroxycarbonate, we explored oxidations in the presence of H_2O_2/**[L$_2$Ni$_4$(CO$_3$)$_2$(H$_2$O)$_2$]$^{2+}$**. Note that this is the same combination of reagents present when **[LNi$_2$(O$_2$CO$_2$)(H$_2$O)$_2$]$^+$** releases H_2O_2 into solution, and no peroxycarbonate is detected when stoichiometric H_2O_2 is added to **[L$_2$Ni$_4$(CO$_3$)$_2$(H$_2$O)$_2$]$^{2+}$** under the reaction conditions.

The same oxidation procedure outlined above was repeated, except solid **[L$_2$Ni$_4$(CO$_3$)$_2$(H$_2$O)$_2$]$^{2+}$** (3.4 mg, 0.002 mmol, 0.5 equiv.) was added in conjunction with the H_2O_2 stock solution. Both a T_0 aliquot and 4-hour aliquot were analyzed to quantify starting material conversion and product formation. Trace oxidation product (sulfoxide) was detected.

13.1% conversion / 0.60% product formation (6.0% relative to H_2O_2)

The slight formation of sulfoxide in both the reactions employing **[LNi$_2$(O$_2$CO$_2$)(H$_2$O)$_2$]$^+$** and H_2O_2/**[L$_2$Ni$_4$(CO$_3$)$_2$(H$_2$O)$_2$]$^{2+}$** inhibits assigning the species responsible for thioether oxidation. Even so, low conversion is observed demonstrating that **[LNi$_2$(O$_2$CO$_2$)(H$_2$O)$_2$]$^+$** is, at best, an ineffective oxidant for this easily oxidized, electron rich substrate.

Isotopic Labeling Experiments

Synthesis of [LNi$_2$(^{13}CO$_3$H)$_2$]$^+$

In the fume hood, a J-Young style NMR tube was charged with **[L$_2$Ni$_4$(CO$_3$)$_2$(H$_2$O)$_2$]$^{2+}$** (6 mg, 0.003 mmol, 1 equiv.) and acetonitrile (*ca.* 600 µL). The tube was subjected to three, freeze/pump/thaw cycles. Upon the final thaw, the tube was backfilled with ^{13}CO$_2$ gas (1 atm). The NMR tube was sealed and mixed via inversion for one hour. The formation of **[LNi$_2$(^{13}CO$_3$H)$_2$]$^+$** was confirmed by ^{1}H NMR spectroscopy, and the reaction solution was used directly for further characterization experiments.

Note: This procedure was concomitantly repeated with unlabeled ^{12}CO$_2$ to yield **[LNi$_2$(^{12}CO$_3$H)$_2$]$^+$** as a means of comparison (product confirmed by ^{1}H NMR spectroscopy).
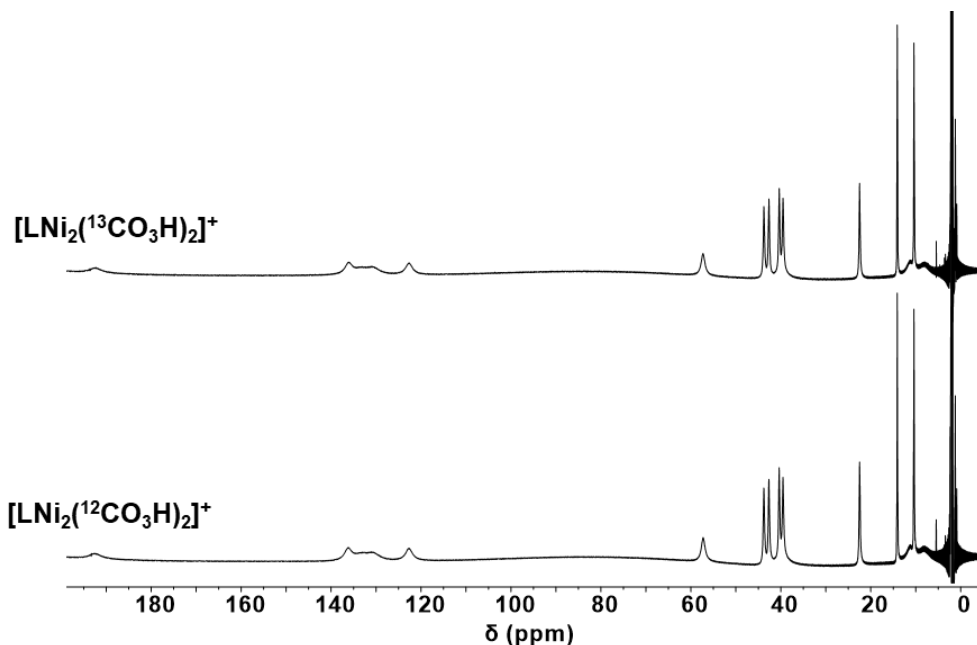
Figure S30. ^{1}H NMR spectra of **[LNi$_2$(^{12}CO$_3$H)$_2$]$^+$** and **[LNi$_2$(^{13}CO$_3$H)$_2$]$^+$** (25 °C, 400 MHz) collected in solvent-suppressed proteo acetonitrile.

Solution State IR of [LNi$_2$(^{13}CO$_3$H)$_2$]$^+$ and [LNi$_2$(^{12}CO$_3$H)$_2$]$^+$

After confirming formation of the bicarbonate isotopologs by NMR spectroscopy (*vide supra*), the acetonitrile solutions of **[LNi$_2$(^{13}CO$_3$H)$_2$]$^+$** and **[LNi$_2$(^{12}CO$_3$H)$_2$]$^+$** were transferred from their respective J. Young NMR tubes to separate 20 mL scintillation vials. A Thermo Nicolet iS50 IR spectrometer equipped with a solution cell holder was blanked by filling the solution cell with benchtop acetonitrile and subtracting the resultant spectrum. The **[LNi$_2$(^{13}CO$_3$H)$_2$]$^+$** and **[LNi$_2$(^{12}CO$_3$H)$_2$]$^+$** solutions were added to the IR cell by pipette (*ca.* 200 µL) and respective spectra were collected for each isotopolog.

Note: The solution IR cell was thoroughly cleaned with acetone and dichloromethane, then dried with N$_2$ gas, between samples to avoid contamination.
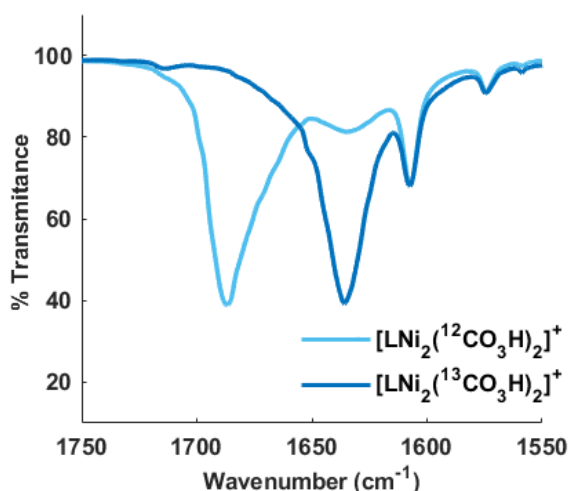
Figure S31. FT-IR spectrum of **[LNi$_2$(^{12}CO$_3$H)$_2$]$^+$** (■) and **[LNi$_2$(^{13}CO$_3$H)$_2$]$^+$** (■) showing a red shift in the C=O stretching frequency of 51 cm^{-1} (37 cm^{-1} calc.) upon ^{13}C isotopic labeling.
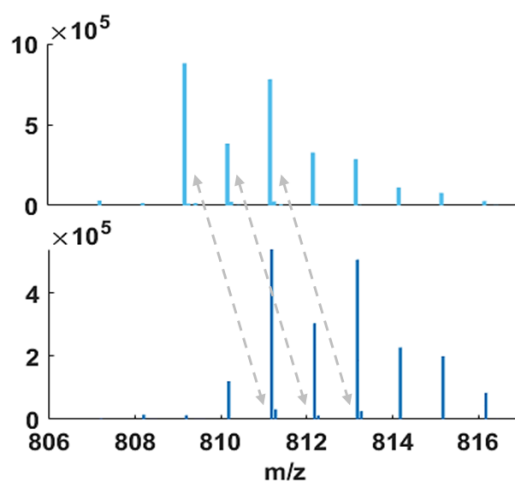
Figure S32. Experimental ESI mass spectra of **[LNi$_2$(^{12}CO$_3$H)$_2$]$^+$** (■) and **[LNi$_2$(^{13}CO$_3$H)$_2$]$^+$** (■) at 25 °C in acetonitrile. The dashed arrows emphasize a 2 m/z unit change corresponding to the incorporation of two ^{13}CO$_2$ molecules per complex.

Synthesis of [LNi$_2$(O$_2$^{13}CO$_2$)(H$_2$O)$_2$]$^+$

In the fume hood, a Schlenk flask was charged with **[L$_2$Ni$_4$(CO$_3$)$_2$(H$_2$O)$_2$]$^{2+}$** (101 mg, 0.06 mmol, 1.0 equiv.), acetonitrile (10 mL), and a magnetic stir bar. It was stoppered with a rubber septum and the pale blue solution was subjected to three freeze/pump/thaw cycles. During the final thaw, the flask was cooled with a dry ice/acetone bath temperature regulated at –30 °C and ^{13}CO$_2$ gas (1 atm) was admitted to the reaction headspace. Immediately after gas addition, a syringe equipped with a disposable needle was used to add H$_2$O$_2$ (50% w/w in water, 630 µL, 11 mmol, 200 equiv.) to the reaction, and the reaction mixture was left to stir for one hour at –30 °C. The reaction was then opened to air, dried with MgSO$_4$, and diethyl ether (*ca.* 6 mL) was added to form a slightly cloudy suspension. Subsequent filtration through Celite afforded a pale purple solution that was stored at –17 °C. After two days, bright purple crystals (27 mg, 0.03 mmol, 26% yield) were collected; the identity of this product was confirmed as pure **[LNi$_2$(O$_2$^{13}CO$_2$)(H$_2$O)$_2$]$^+$** by ^{1}H NMR spectroscopy.
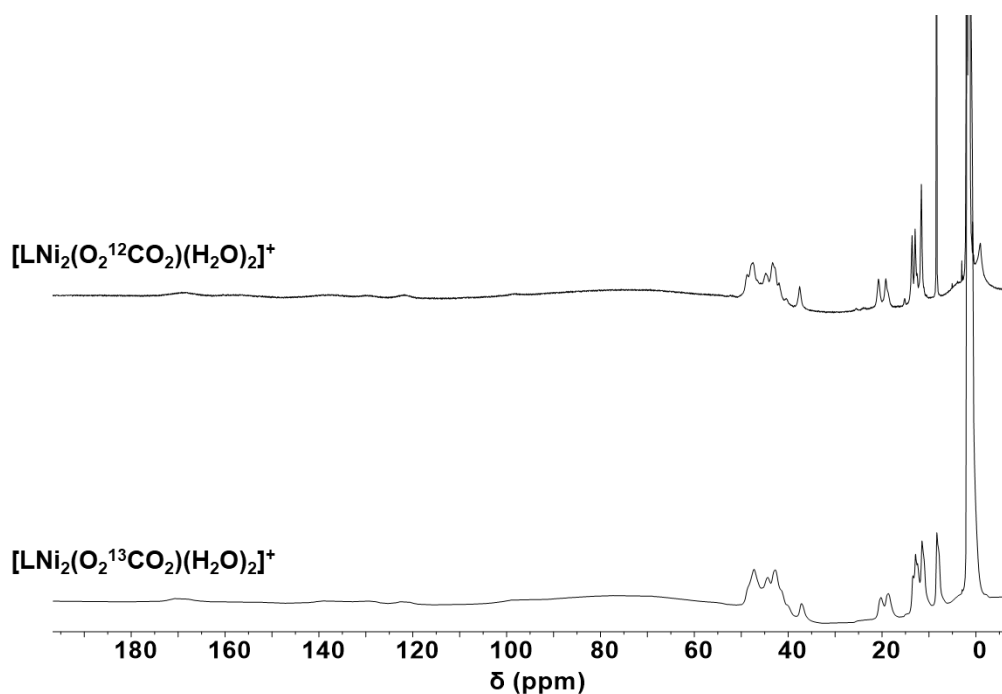
Figure S33. Stacked ^{1}H NMR spectra comparing crystalline samples of **[LNi$_2$(O$_2$^{12}CO$_2$)(H$_2$O)$_2$]$^+$** and **[LNi$_2$(O$_2$^{13}CO$_2$)(H$_2$O)$_2$]$^+$** (acetonitrile, –25 °C, 500 MHz).

$^{13}C\{^1H\}$ NMR Experiment to Monitor the Decomposition of $[LNi_2(O_2^{13}CO_2)(H_2O)_2]^+$

Crystalline $[LNi_2(O_2^{13}CO_2)(H_2O)_2]^+$ (15 mg, 0.016 mmol, 1 equiv.) was dissolved in CD_3CN pre-cooled to –30 °C in a J. Young style NMR tube. The tube was introduced to an NMR spectrometer with the probe pre-cooled to –25 °C. $^{13}C\{^1H\}$ NMR spectra were collected at temperature increments beginning at –25 °C and ending at 25 °C (corroborated with ^1H NMR spectra at the beginning and end of the temperature range).
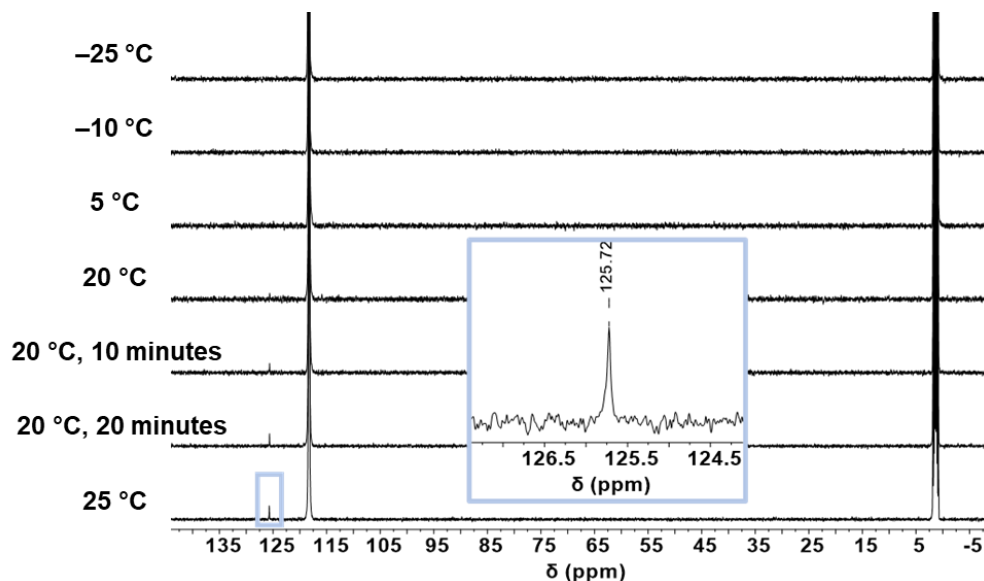
Figure S34. $^{13}C\{^1H\}$ NMR spectra (CD_3CN, 126 MHz) of $[LNi_2(O_2^{13}CO_2)(H_2O)_2]^+$ at temperatures ranging from –25 °C to 25 °C. Each trace is labeled with its corresponding temperature; the reaction was held at the stated temperature for approximately 2 minutes unless otherwise noted. Starting at 20 °C, free $^{13}CO_2$ (125.72 ppm) (☐) is observed, consistent with non-negligible decomposition upon conversion of $[LNi_2(O_2^{13}CO_2)(H_2O)_2]^+$ to $[L_2Ni_4(CO_3)_2(H_2O)_2]^{2+}$. **Inset:** Expansion of free $^{13}CO_2$ spectral feature at 25 °C.

Note: Given that the peroxycarbonate complex, $[LNi_2(O_2^{13}CO_2)(H_2O)_2]^+$, decomposes more rapidly than free $^{13}CO_2$ is observed to grow in, we cannot conclusively rule out further degradation of $[L_2Ni_4(CO_3)_2(H_2O)_2]^{2+}$ in the reaction mixture. These data are consistent with sub-unity phosphine oxide yields (*cf.* **Figure S24**) and the byproducts observed in ^1H NMR experiments (*cf.* **Figure S23**) described in detail above.

Crystallographic Information

CCDC deposition numbers 2348000 – 2348003 contain the supplementary crystallographic data for this paper. These data can be obtained free of charge from The Cambridge Crystallographic Data Centre via www.ccdc.cam.ac.uk/data_request/cif.

Refinement Details

In each case, crystals were mounted on a MiTeGen loop, using Paratone oil, then placed on a Rigaku AFC10K Saturn 944+ CCD-based X-ray diffractometer equipped with a low temperature cryostream and a Mircomax-007HF Cu-target micro-focus rotating anode (λ = 1.54187 Å) operated at 1.2 kW power (40 kVm 30 mA). The X-ray intensities were measured at 85(1) K or 120(1) K with the detector located at a distance of 42.00 mm from the crystal. Rigaku d*trek images were exported to CrysAlisPro[8] for processing and corrected for absorption using spherical harmonics, as implemented in the SCALE3 ABSPACK scaling algorithm.[9] Space groups were determined on the basis of systematic absences and intensity statistics and the structures were solved using SHELXTL intrinsic phasing (XT)[10] as incorporated into the Olex2 software interface.[11] Solutions were refined (SHELXL)[12] by full-matrix least squares on F^2 to convergence. All non-hydrogen atoms were refined using anisotropic displacement parameters and hydrogen atoms were placed in the idealized positions and refined using a riding model, unless noted otherwise. Graphical representations of structures with 50% probability thermal anisotropic displacement ellipsoids were generated as Posctscript vector images via Olex2.

Note Regarding Missing Reflections: The diffractometer employed in these studies is a protein system that has been adapted for small molecule use. There are two specific defects in this retrofitting that lead to missing reflections in the datasets. The first is a limitation of –70/+70 degrees in kappa, stemming from the instrument hardware. The effects of this kappa limitation on data completeness are particularly significant in the datasets of triclinic crystals. The second major issue is a missing attenuator for the CCD camera; this leads to frequent reflection overloads that also contributes to missing reflections in the collected datasets.

Table S1—Crystal and refinement data for **[LNi₂(OTf)₂][OTf]**, **[L₂Ni₄(CO₃)₂(H₂O)₂][OTf]₂**, **[L₂Ni₄(OH)₄][OTf]₂**, and **[LNi₂(O₂CO₂)(H₂O)₂][OTf]**

	[LNi$_2$(OTf)$_2$][OTf]	[L$_2$Ni$_4$(CO$_3$)$_2$(H$_2$O)$_2$][OTf]$_2$	[L$_2$Ni$_4$(OH)$_4$][OTf]$_2$	[LNi$_2$(O$_2$CO$_2$)(H$_2$O)$_2$][OTf]
CCDC Number[13]	2348000	2348002	2348003	2348001
Internal Reference Code	cp125	hl524	hll273	hll169
Empirical formula	C$_{40}$H$_{41}$Cl$_2$F$_9$N$_6$Ni$_2$O$_{10}$S$_3$	C$_{76}$H$_{93}$F$_6$N$_{12}$Ni$_4$O$_{21.5}$S$_2$	C$_{86}$H$_{106}$F$_6$N$_{12}$Ni$_4$O$_{15}$S$_2$	C$_{38}$H$_{57}$F$_3$N$_6$Ni$_2$O$_{17}$S
Formula weight	1221.29	1931.58	1960.78	1076.37
T (K)	85	85	85	85
a, Å	11.11800(1)	16.1401(9)	13.7338(4)	10.2519(3)
b, Å	20.66740(1)	32.5762(9)	18.9753(5)	11.2496(4)
c, Å	21.7121(2)	17.5728(6)	33.7970(12)	21.4920(7)
α, °	90	90	90	77.624(3)
β, °	98.029(1)	111.887(5)	90	79.248(3)
γ, °	90	90	90	80.429(3)
Volume, Å^3	4940.1(1)	8573.5(7)	8807.6(5)	2357.9(1)
Z	4	4	4	2
Crystal system	monoclinic	monoclinic	orthorhombic	triclinic
Space group	P2$_1$/n	P2$_1$/c	P2$_1$2$_1$2$_1$	P-1
d_{calc}, g/cm^3	1.642	1.420	1.316	1.516
2θ range, °	5.932 to 138.858	5.426 to 139.29	5.23 to 140.306	4.262 to 139.364
μ, mm^{-1}	3.975	2.137	2.016	2.175
Abs. Correction	Multi-scan	Multi-scan	Multi-scan	Multi-scan
GOF	1.114	1.020	1.049	1.056
R_1,^{a} wR_2^{b} [I>2 σ(I)]	R$_1$ = 0.0442, wR$_2$ = 0.1100	R$_1$ = 0.1343, wR$_2$ = 0.3495	R1 = 0.0795, wR2 = 0.2111	R1 = 0.0798, wR2 = 0.2200
Radiation Type	Cu Kα (λ = 1.54184)	Cu Kα (λ = 1.54178)	Cu Kα (λ = 1.54178)	Cu Kα (λ = 1.54184)

^{a} R$_1$ = ∑||F$_o$| - |F$_c$||/∑|F$_o$|. ^{b} wR$_2$ = [∑[w(F$_o$^{2}-F$_c$^{2})^2]/∑[w(F$_o$^{2})^2]$^{1/2}$

Structural Determination of [LNi₂(OTf)₂][OTf]

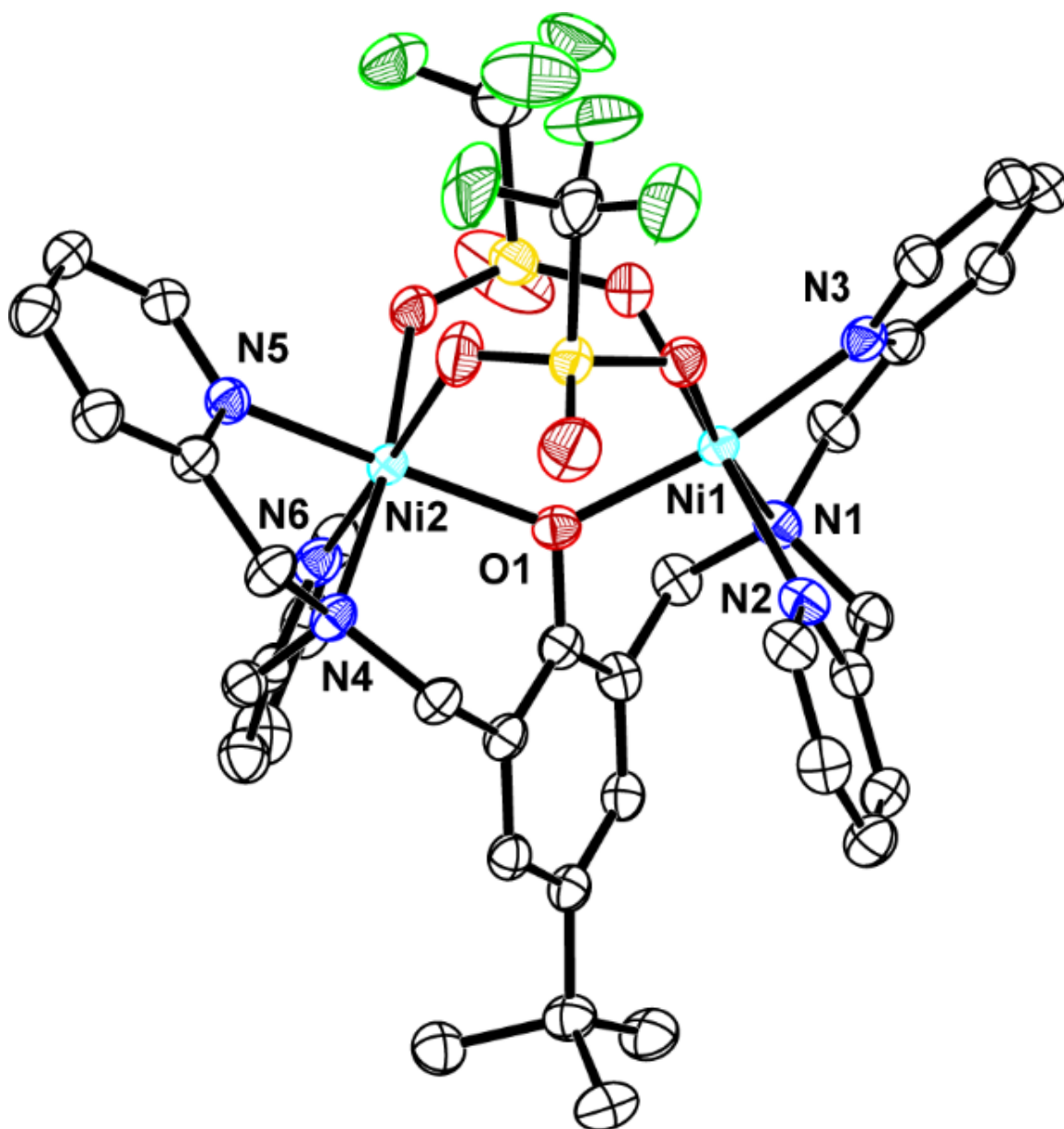**Figure S35 –** Structural drawing of **[LNi₂(OTf)₂][OTf]** with 50% probability anisotropic displacement ellipsoids. H-atoms and the trifluoromethanesulfonate counterion are omitted for clarity.

Special Refinement Details: The tert-butyl group of the bicompartmental ancillary ligand (C7 > C10) suffered from positional disorder that was modeled satisfactorily over two discrete positions in an 82:18 population ratio. Additionally, a dichloromethane solvate molecule (Cl1 Cl2 C40; from the crystallization medium) was present and showed partial disorder of the central carbon (C40) and one of the two chlorides (Cl2). This was modeled satisfactorily in a 74:26 population ratio with 1,2- and 1,3-similarity restraints and enhanced rigid bond restraints; the components of the displacement parameters along the bond axis are restrained to be equivalent.

Structural Determination of [L₂Ni₄(CO₃)₂(H₂O)₂][OTf]₂
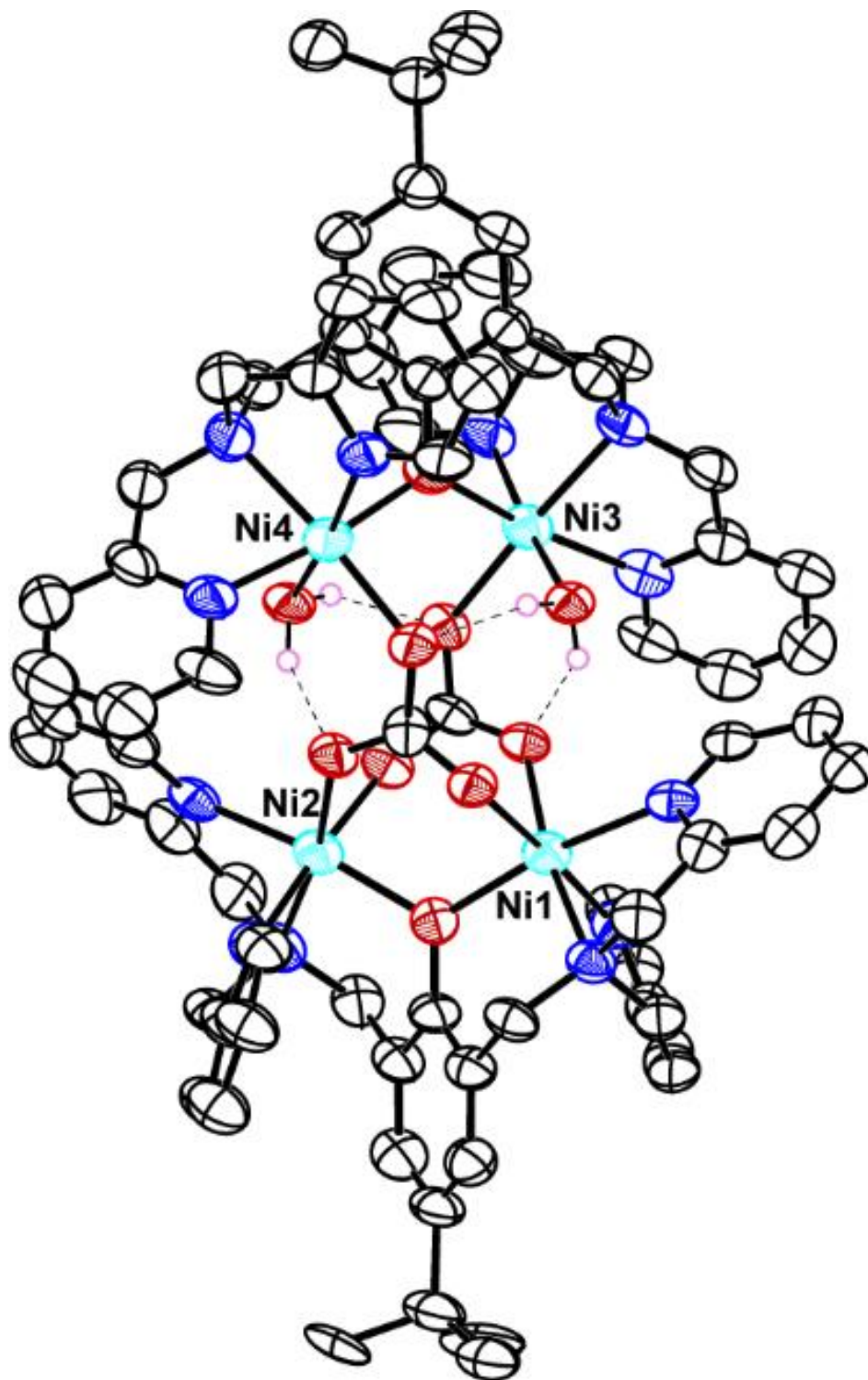
Figure S36 – Full Structural drawing of **[L₂Ni₄(CO₃)₂(H₂O)₂][OTf]₂** with 50% probability anisotropic displacement ellipsoids. H-atoms (except those of the bound aquo ligands) and the trifluoromethanesulfonate counterions are omitted for clarity.
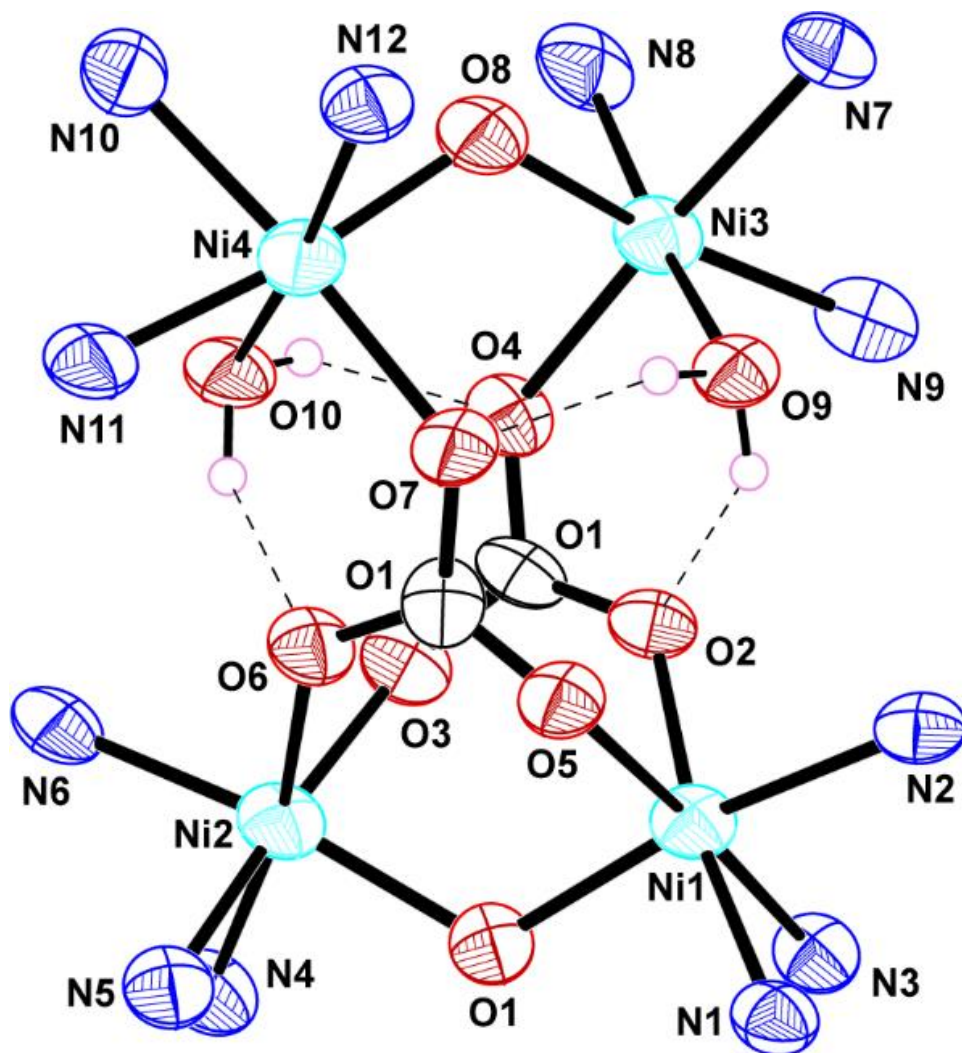
Figure S37 – Truncated Core Structure of **[L$_2$Ni$_4$(CO$_3$)$_2$(H$_2$O)$_2$][OTf]$_2$** with 50% probability anisotropic displacement ellipsoids. C and H atoms of the ancillary ligand and the trifluoromethanesulfonate counterions are omitted for brevity.

Special Refinement Details: The tert-butyl group of one of the two bicompartmental ancillary ligands (C7 > C10) suffered from positional disorder that was modeled satisfactorily over two discrete positions in a 72:28 population ratio with both 1,2- and 1,3-distance similarity restraints and enhanced rigid bond restraints. The trifluoromethanesulfonate counterions suffered from positional disorder and were modeled with idealized fragments from Ilia Guzei's Fragment Database[14] as implemented in the Olex2 user interface. These idealized fragments were modeled over two discrete positions for each triflate anion—in population ratios of 80:20 and 75:25 for S1 O11 > O13 C75 F1 > F3 and S2 O14 > O16 C76 F4 > F6, respectively. Finally, the large size of the primary residue generates large solvent accessible voids in the crystal lattice that contained hydrogen bonding networks of water solvate molecules. BYPASS was implemented to account for the residual solvent electron density. A solvent mask was calculated and 236 electrons were found in a volume of 1052 Å^3 in two voids per unit cell. This is consistent with the presence of 5.5 water [H$_2$O] molecules per asymmetric unit, which account for 220 electrons per unit cell.

Structural Determination of [L₂Ni₄(OH)₄][OTf]₂
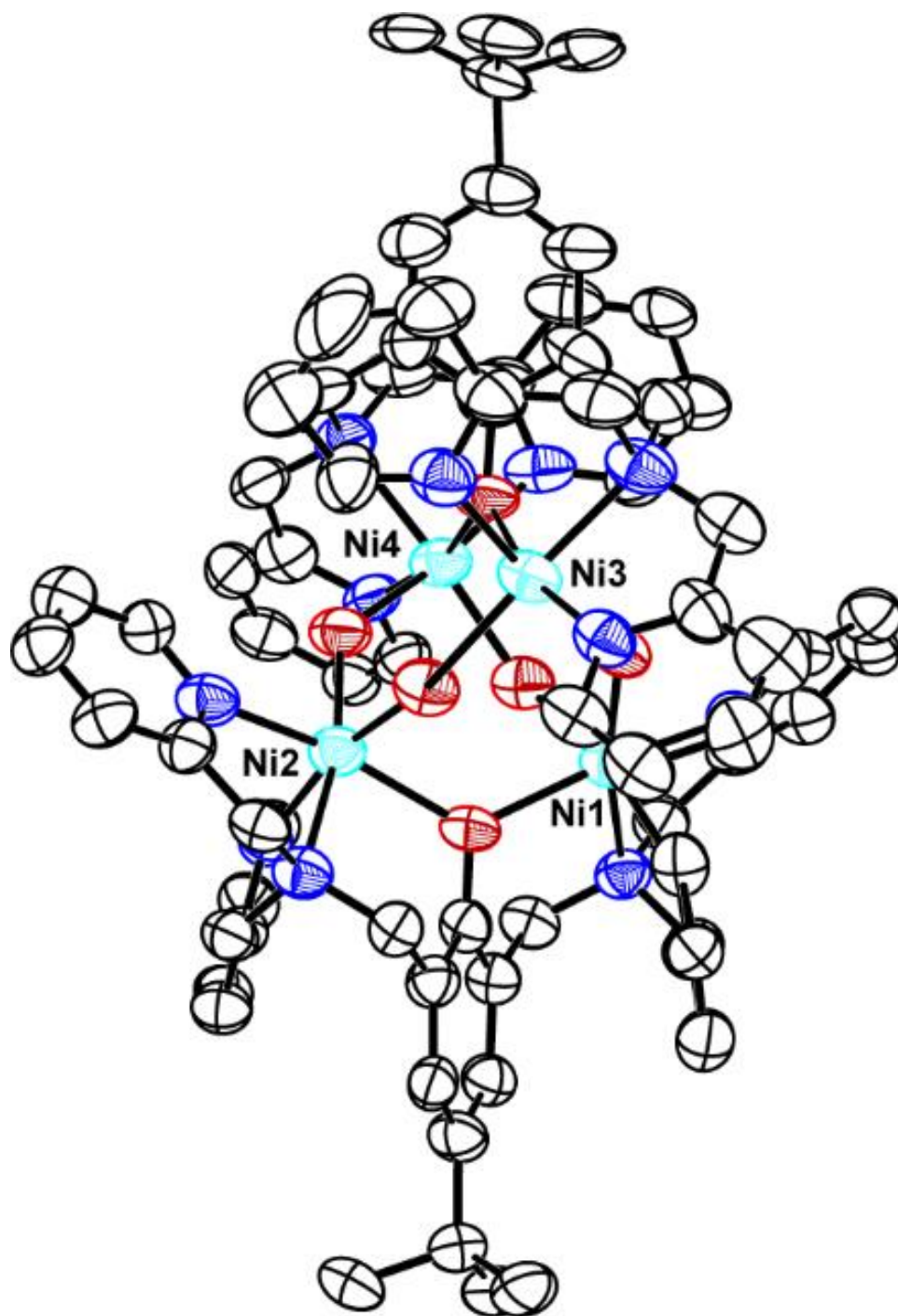
Figure S38 – Full Structural drawing of **[L₂Ni₄(OH)₄][OTf]₂** with 50% probability anisotropic displacement ellipsoids. H-atoms and the trifluoromethanesulfonate counterions are omitted for clarity.
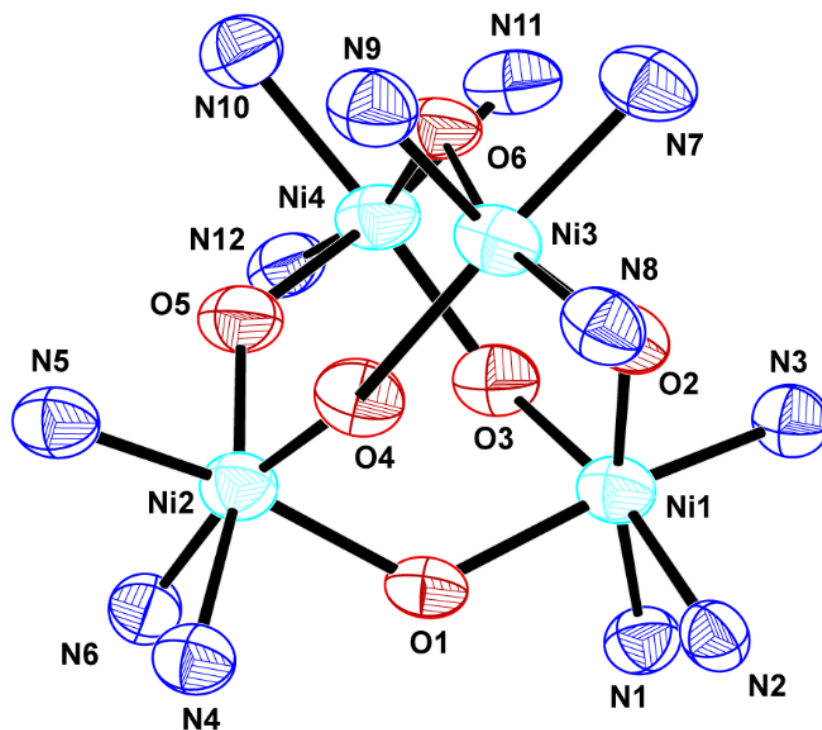
Figure S39 – Truncated Core Structure of **[L$_2$Ni$_4$(OH)$_4$][OTf]$_2$** with 50% probability anisotropic displacement ellipsoids. C and H atoms of the ancillary ligand and the trifluoromethanesulfonate counterions are omitted for brevity.

Special Refinement Details: The tert-butyl group of one of the two bicompartmental ancillary ligands (C43 > C46) suffered from positional disorder that was modeled satisfactorily over two discrete positions in a 56:44 population ratio. Both disordered components were modeled with 1,2- and 1,3-similarity restraints and enhanced rigid bond restraints. Given the poor quality of the dataset, the hydroxide hydrogen atoms were not discernable in the Fourier map. To model these, H-atoms were placed 0.990 Å from each μ–O (O2 > O5) and treated with 1,3-distance (angle distance) restraints. The combination of these restraints afforded chemically reasonable geometries and stable refinement for the four H-atoms of the μ-OH ligands. The two triflate anions were likewise disordered. The first, S1 O7 > O9 C48 F1 > F3, was modeled over two discrete positions (87:13) with both 1,2- and 1,3-distance similarity restraints. Strong enhanced rigid bond restraints were required for the minor component to refine stably, given the proximity of the overlapping atoms. The second triflate, S2 O10 > O12 C49 F4 > F6, likewise suffered from a positional disorder with two major components (58:42) and was modeled with idealized fragments from Ilia Guzei's Fragment Database[14] as implemented in the Olex2 user interface.

Structural Determination of [LNi$_2$(O$_2$CO$_2$)(H$_2$O)$_2$][OTf]
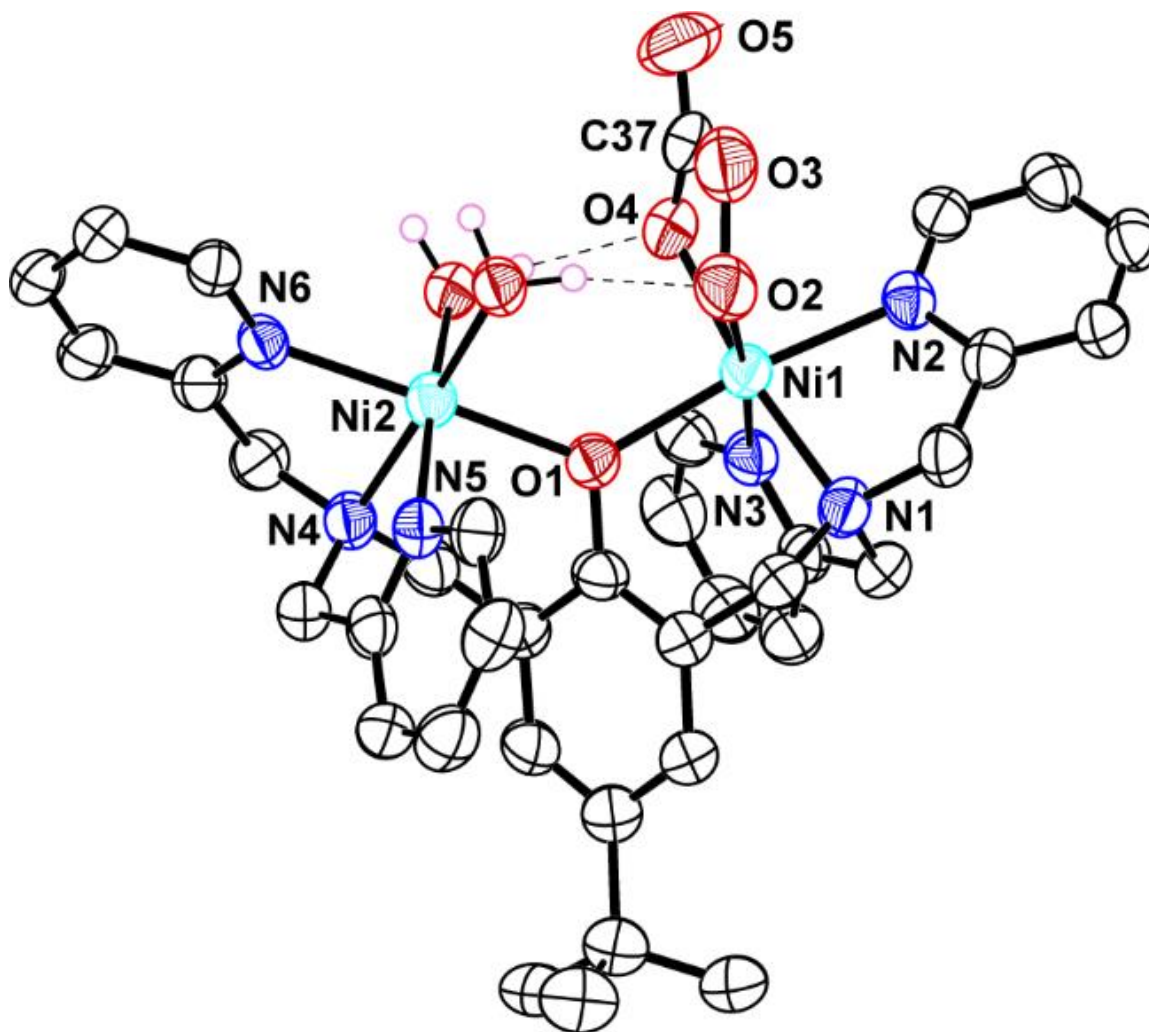
Figure S40 – Structural drawing of **[LNi$_2$(O$_2$CO$_2$)(H$_2$O)$_2$][OTf]** with 50% probability anisotropic displacement ellipsoids. H-atoms (except those of the bound aquo ligands) and the trifluoromethanesulfonate counterion are omitted for clarity.

Special Refinement Details: The tert-butyl group of the bicompartmental ancillary ligands (C7 > C10) suffered from positional disorder that was modeled satisfactorily over two discrete positions in a 77:23 population ratio. Both disordered components were modeled with 1,2- and 1,3-similarity restraints and enhanced rigid bond restraints. Additionally, as these crystals were grown in benchtop solvent, a hydrogen bonding network of solvate water molecules was present in the lattice. BYPASS was implemented to account for the residual solvent electron density. A solvent mask was calculated and 124 electrons were found in a volume of 456 Å^3 in one void per unit cell. This is consistent with the presence of six water [H$_2$O] molecules per asymmetric unit, which account for 120 electrons per unit cell.

References

(1)   A. B. Pangborn; M. A. Giardello; R. H. Grubbs; R. K. Rosen; F. J. Timmers, *Organometallics*, 1996, **15**, 1518

(2)   N. E. Dixon, G. A. Lawrance, P. A. Lay, A. M. Sargeson, and H. Taube. Introduction to Trifluoromethanesulfonates and Trifluoromethanesulfonato-*O* Complexes. In Inorganic Syntheses, J.M. Shreeve (Ed.). John Wiley & Sons: New York, 1986, 243-250.

(3)   G. R. Fulmer; A. J. M. Miller; N. H. Sherden; H. E. Gottlieb; A. Nudelman; B. M. Stoltz; J. E. Bercaw; K. I. Goldberg, *Organometallics*, 2010, **29**, 2176

(4)   C. Su; Z. Chen; Q. Feng; F. Wei; A. Mo; H.-H. Huang; H. Hu; H. Zou; F. Liang; D. Liu, *Dalton Trans.*, 2023, **52**, 4548

(5)   M. P. Crockett; H. Zhang; C. M. Thomas; J. A. Byers, *Chem. Commun.*, 2019, **55**, 14426

(6)   T. Tsugawa; H. Furutachi; M. Marunaka; T. Endo; K. Hashimoto; S. Fujinami; S. Akine; Y. Sakata; S. Nagatomo; T. Tosha; T. Nomura; T. Kitagawa; T. Ogura; M. Suzuki, *Chem. Lett.*, 2014, **44**, 330

(7)   M. Matteucci; G. Bhalay; M. Bradley, *Org. Lett.*, 2003, **5**, 235

(8)   Agilent (2022). CrysAlis^{Pro} Software System, version 1.171.42.61a. Agilent Technologies UK Ltd, Oxford, UK.

(9)   SCALE3 ABSPACK - An Oxford Diffraction program (1.0.4,gui:1.0.3) (C) 2005 Oxford Diffraction Ltd.

(10)   G. Sheldrick, *Acta Cryst. A*, 2015, **71**, 3

(11)   O. V. Dolomanov; L. J. Bourhis; R. J. Gildea; J. A. K. Howard; H. Puschmann, *J. Appl. Crystallogr.*, 2009, **42**, 339

(12)   G. Sheldrick, *Acta Cryst. C*, 2015, **71**, 3

(13)   Crystallographic data have been deposited at the CCDC, 12 Union Road, Cambridge CB2 1EZ, UK and copies can be otained on request, free of charge, by quoting the publication citation and the respective deposition numbers.

(14)   I. Guzei, *J. Appl. Crystallogr.*, 2014, **47**, 806